COHERENT OPTICAL ADAPTIVE TECHNIQUES (COAT)

W. B. Bridges, et al

Hughes Research Laboratories

Prepared for:

Rome Air Development Center
Advanced Research Projects Agency

April 1974

UNCLASSIFIED

SECURITY CLASSIFICATION OF THIS PAGE (When Data Entered)

REPORT DOCUMENTATION PAGE

READ INSTRUCTIONS BEFORE COMPLETING FORM

1. REPORT NUMBER: RADC-TR-74-187	2. GOVT ACCESSION NO.
3. RECIPIENT'S CATALOG NUMBER: AD 783281	
4. TITLE (and Subtitle): Coherent Optical Adaptive Techniques (COAT)	5. TYPE OF REPORT & PERIOD COVERED: Interim 27 Dec 73 to 26 Mar 74
	6. PERFORMING ORG. REPORT NUMBER: Tech. Report # 4
7. AUTHOR(s): W.B. Bridges, L.S. Horwitz, R.M. Kubo, J.E. Pearson, T.J. Walsh	8. CONTRACT OR GRANT NUMBER(s): F30602-73-C-0248
9. PERFORMING ORGANIZATION NAME AND ADDRESS: Hughes Research Lab, 3011 Malibu Canyon Rd., Malibu, Calif. 90265	10. PROGRAM ELEMENT, PROJECT, TASK AREA & WORK UNIT NUMBERS: 62301E, 12790016
11. CONTROLLING OFFICE NAME AND ADDRESS: Defense Advanced Research Projects Agency, 1400 Wilson Blvd, Arlington, Va. 22209	12. REPORT DATE: April 1974
	13. NUMBER OF PAGES: 58
14. MONITORING AGENCY NAME & ADDRESS(if different from Controlling Office): Rome Air Development Center (OCTM), ATTN: Robert F. Ogrodnik, Griffiss AFB NY 13441	15. SECURITY CLASS. (of this report): Unclassified
	15a. DECLASSIFICATION/DOWNGRADING SCHEDULE

16. DISTRIBUTION STATEMENT (of this Report)

Approved for public release. Distribution unlimited.

17. DISTRIBUTION STATEMENT (of the abstract entered in Block 20, if different from Report)

Approved for public release. Distribution unlimited.

18. SUPPLEMENTARY NOTES

19. KEY WORDS (Continue on reverse side if necessary and identify by block number)

Laser Phased Array
Adaptive Aperture
Atmospheric Turbulence Compensation

20. ABSTRACT (Continue on reverse side if necessary and identify by block number)

Coherent optical adaptive techniques are designed to overcome degradations experienced by optical beams propagating in media with fixed or time-varying distortions. This report presents results from the calibration phase of an experimental eighteen-element, self-adaptive optical phased array. Initial tests on a turbulent, outdoor propagation range are also presented. Computer simulation studies have demonstrated the advantages of a divider-AGC network (continued)

DD FORM 1 JAN 73 1473 EDITION OF 1 NOV 65 IS OBSOLETE

UNCLASSIFIED

SECURITY CLASSIFICATION OF THIS PAGE (When Data Entered)

Item 20: Abstract (continued)

and have detailed the theoretical system performance with glints of varying reflectivities, with various signal-to-noise ratios, and with different receiver aperture diameters. Phase shifter hysteresis was found to have a negligible effect on system performance. Laboratory calibration measurements both with and without artificial turbulence show that the experimental COAT system performs very close to theoretical predictions. Initial range measurements with high turbulence ($C_N^2 = 6 \times 10^{-15}$ $cm^{-2/3}$) show very good system lock-on convergence (5 ms convergence time) and stability ($\pm$ 10% intensity fluctuations) with a single moving glint target.

COHERENT OPTICAL ADAPTIVE TECHNIQUES (COAT)

W. B. Bridges
L. S. Horwitz
R. M. Kubo
J. E. Pearson
T. J. Walsh

Contractor: Hughes Aircraft Company
Contract Number: F30602-73-C-0248
Effective Date of Contract: 27 March 1973
Contract Expiration Date: 30 June 1974
Amount of Contract: $307,692.00
Program Code Number: 3E20

Principal Investigator: W. B. Bridges
Phone: 213 456-6411

Project Engineer: Robert F. Ogrodnik
Phone: 315 330-4306

Contract Engineer: Robert Hawkins
Phone: 315 330-4731

Approved for public release;
distribution unlimited.

This research was supported by the Defense Advanced Research Projects Agency of the Department of Defense and was monitored by Robert F Ogrodnik, RADC (OCTM) GAFB NY 13441 under Contract F30602-73-C-0248, Job Order No. 12790016.

FOREWORD

This quarterly report was prepared by Hughes Research Laboratories, Malibu, California, under Contract No. F30602-73-C-0248. It describes work performed from 27 December 1973 to 26 March 1974. The principal investigator and principal scientist is Dr. William B. Bridges.

This report has been reviewed by the RADC Information Office, OI, and is releasable to the National Technical Information Service (NTIS).

This technical report has been reviewed and is approved.

Robert F. Ogrodnik

ROBERT F. OGRODNIK

ABSTRACT

Coherent optical adaptive techniques are designed to overcome degradations experienced by optical beams propagating in media with fixed or time-varying distortions. This report presents results from the calibration phase of an experimental eighteen-element, self-adaptive optical phased array. Initial tests on a turbulent, outdoor propagation range are also presented. Computer simulation studies have demonstrated the advantages of a divider-AGC network and have detailed the theoretical system performance with glints of varying reflectivities, with various signal-to-noise ratios, and with different receiver aperture diameters. Phase shifter hysteresis was found to have a negligible effect on system performance. Laboratory calibration measurements both with and without artificial turbulence show that the experimental COAT system performs very close to theoretical predictions. Initial range measurements with high turbulence ($C_N^2 = 6 \times 10^{-15}$ $cm^{-2/3}$) show very good system lock-on convergence (5 ms convergence time) and stability (±10% intensity fluctuations) with a single moving glint target.

SUMMARY

This report covers the period of 27 December 1973 to 26 March 1974, the fourth quarter of the contract. During the quarter, we completed the construction and testing of all the necessary hardware for the COAT system, the target, and the range. The visible prototype COAT system is now operating on the outdoor propagation range at Hughes Ground Systems Group facility.

Studies using the COAT computer simulation have continued. We have verified the improvement in system performance when using a divider-AGC network. Convergence tests with two glints have shown that the system will always converge completely and remain converged on one glint, but the glints must differ by at least 1 dB for the system to consistently pick the stronger glint. This conclusion remains true for voltage signal-to-noise ratios above 6. Initial tests with varying receiver aperture sizes and areas have shown no effect for receiver diameters as small as one-third the transmitter diameter. The simulation has also shown that phase shifter hysteresis has very little detrimental effect on convergence performance.

Laboratory calibration performance tests on the COAT system have been completed using the 18-element 0-6-12 transmitter array. The system performs very close to computer-predicted theoretical levels in tests of convergence times, target plane intensity contours, and glint discrimination. Laboratory measurements indicate that two glints must differ in reflectivity by 2 dB for the COAT system to converge completely on the stronger one.

Initial range measurements have shown stable system convergence with a single stationary or moving glint at turbulence levels up to $C_N^2 = 6 \times 10^{-15}$ cm$^{-2/3}$. The turbulence was measured with a differential microthermometer. Convergence times are typically 5 ms with only 5 to 10% peak intensity fluctuations after convergence. Peak-to-peak phase shifter excursions after convergence are roughly $\pm 118^\circ$ or 0.16 μm. Mechanical offset-pointing under turbulent conditions has been demonstrated, but its usefulness is limited by mirror bounce requiring long sample times.

TABLE OF CONTENTS

LIST OF ILLUSTRATIONS

I. INTRODUCTION

A. Program Objectives

There are two primary objectives of this program. The first objective is to determine the performance limits of coherent optical adaptive techniques through operation of an experimental, visible prototype multi-dither COAT system through a representative turbulent atmosphere against a complex dynamic target. The second objective is to determine the best methods of employing COAT in high power laser systems and to assess the status of necessary key high power components.

B. Research Program Plan

The research program plan is the same as that presented in the previous technical report.[1] The program ends June 30, 1974. Final range test data and the results of Task III, the high-power COAT study, will be presented in the final contract report due in July, 1974. Figure 1 shows the test and measurements program for the entire contract.

C. Organization of This Report

This report covers the end of the calibration phase and the beginning of the range measurements phase of the contract. Results obtained during the time period of 27 December 1973 to 26 March 1974 are included.

The report is divided into six sections. Section II discusses recent computer simulation results on signal-to-noise, glint discrimination, and effects of receiver size and phase-shifter hysteresis. The improvement in system performance after the inclusion of a divider-AGC is also noted.

Section III presents the operational status of the target and range analysis equipment. A new TV camera has been purchased to facilitate calibrated target measurements.

Section IV contains the final laboratory calibration measurements data for the 18-element COAT system. Near-ideal performance was observed and the dynamic system operation recorded on movie film.

Section V presents the results of preliminary range measurements which show good system convergence performance under high turbulence conditions. The report concludes with Section VI outlining the plans for the final quarter of the program.

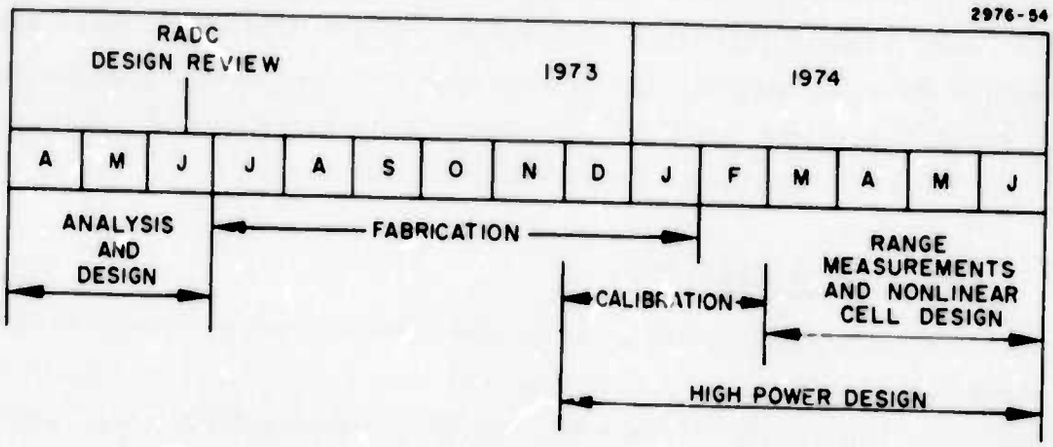

Fig. 1. COAT test and measurements program.

II. ANALYSIS: COMPUTER SIMULATION STUDIES

A. Simulation Modifications

During this quarter we have solved the difficulties experienced in incorporating the divider AGC into the simulation. The optimum corner frequency for the low-pass filter in the AGC was found to be about 4 kHz, but system performance is nearly constant for any corner frequency between 500 Hz and 8 kHz. The value presently in use in the hardware is 2 kHz.

The effect of the AGC is to produce fast, reliable convergence with all glint geometries studied so far, but the maximum converged power is about 10% below that obtained with no AGC and optimum gain. This is not a surprising result, since the AGC reduces the gain as convergence proceeds and the final converged level is proportional to loop gain. This small reduction is more than compensated, however, by increased stability and reduced convergence time particularly with moving, multiglint targets.

All of the simulation tests reported here were run with sine/cosine operation and a signal-to-noise (S/N) of 20 unless otherwise noted. The S/N ratio is defined as the ratio of the detector dc voltage to the rms signal shot noise voltage. The loop gain was optimized for fastest stable convergence on a single glint with the AGC and then left unchanged for all tests.

B. Two Glint Discrimination

Two questions of great practical importance are the following: (1) How does the COAT system behave with the two equal glints? (2) By how much must two glints differ for the COAT system to always choose the stronger? A number of simulation tests were made to answer these questions.

1. Two Identical, Resolvable Glints

For these tests, two equal, resolvable glints were placed on the x-axis equal distances from the boresight axis. Three tests were run with different glint spacings using the initial condition shown in Fig. 2. The results are given in Figs. 3 through 5, where both the target plane power plots and the glint power time history plots are shown. The glint spacing

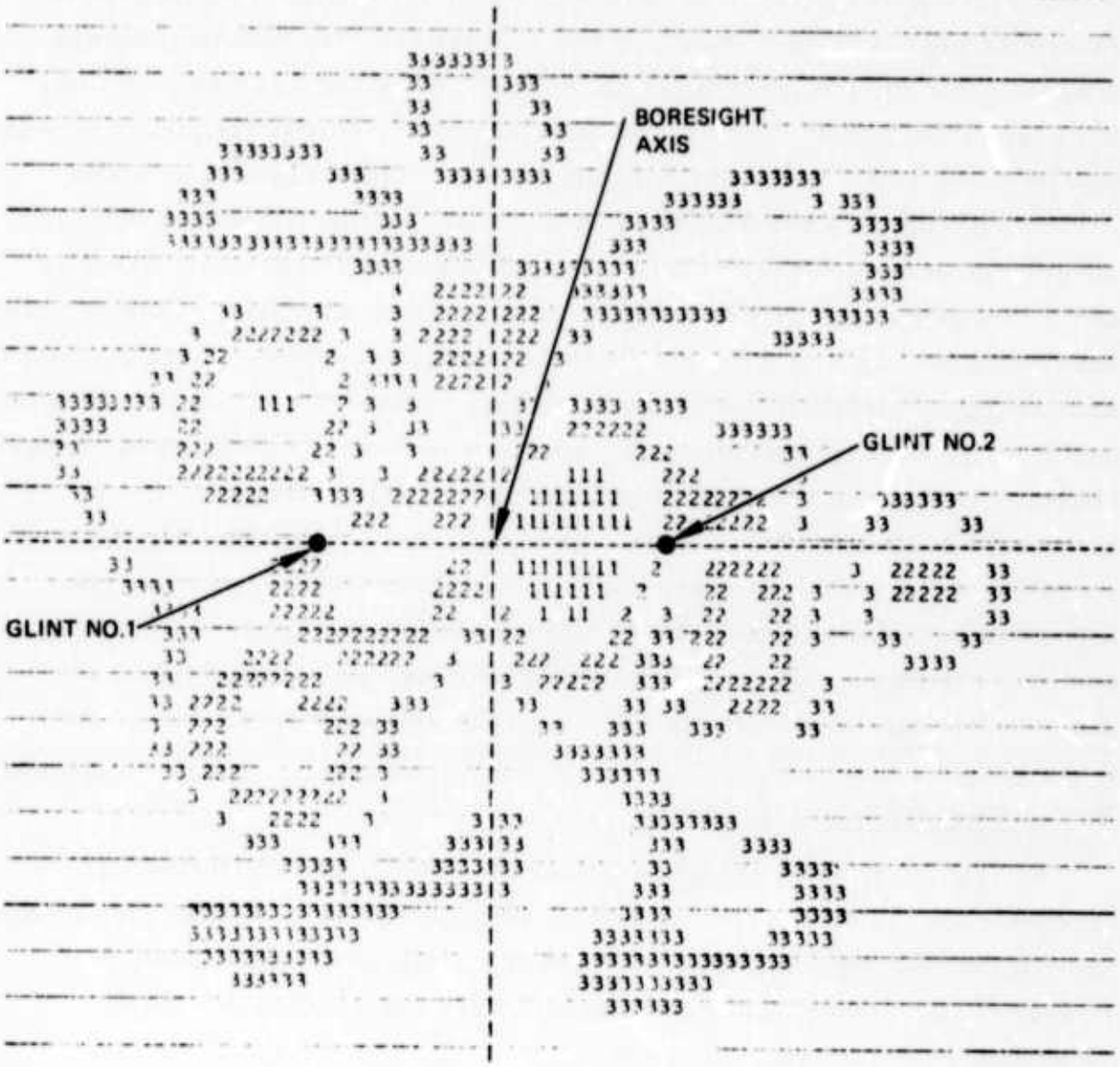

Fig. 2. Target plane power plot showing initial condition for identical, resolvable glint tests. Glints are shown spaced at one-fourth of an element null-null beamwidth.

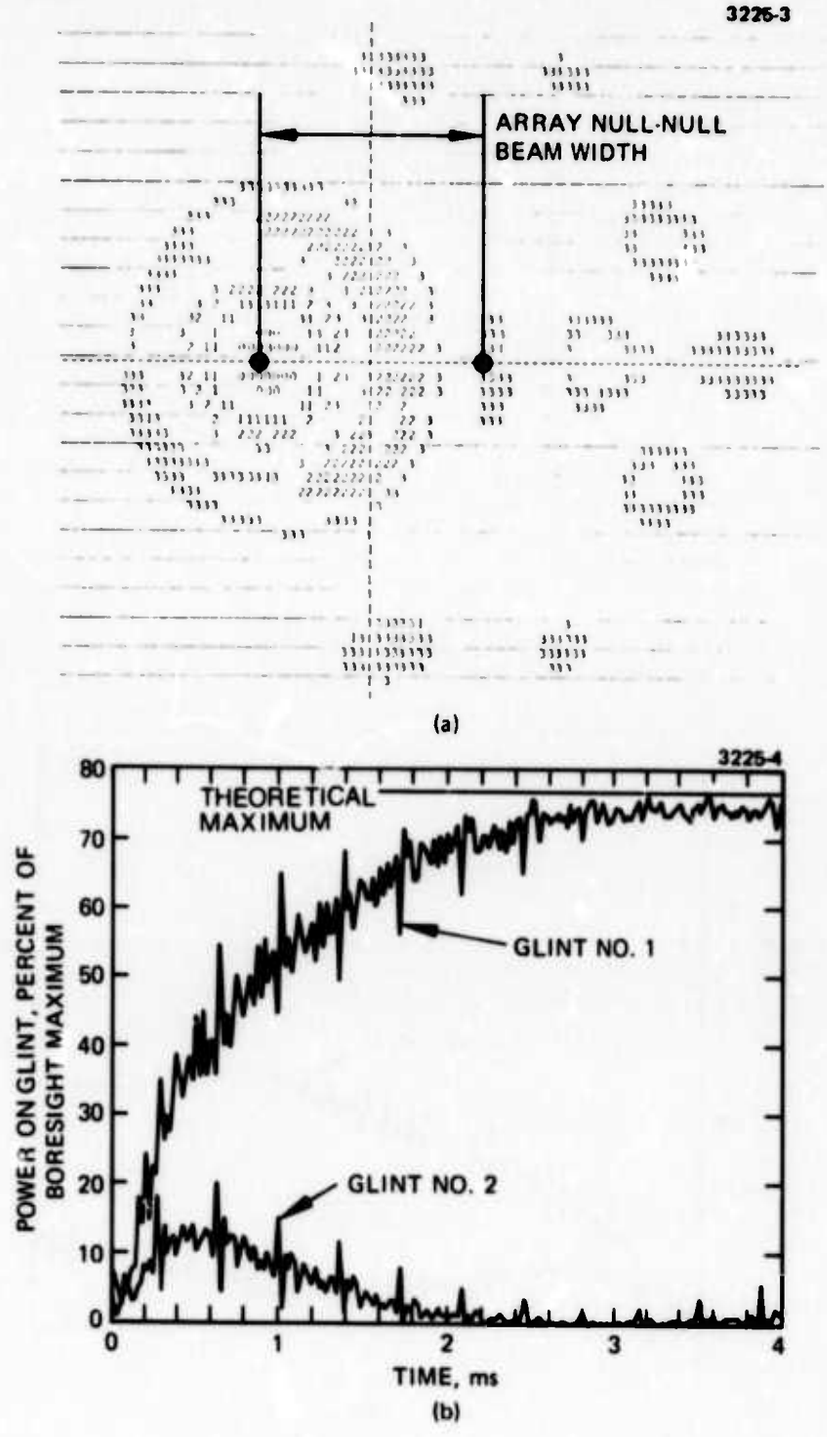

Fig. 3. Convergence run for two equal glints spaced at one array null-null beamwidth. (a) Converged pattern after 4 msec. (b) Time history plot of power on each glint.

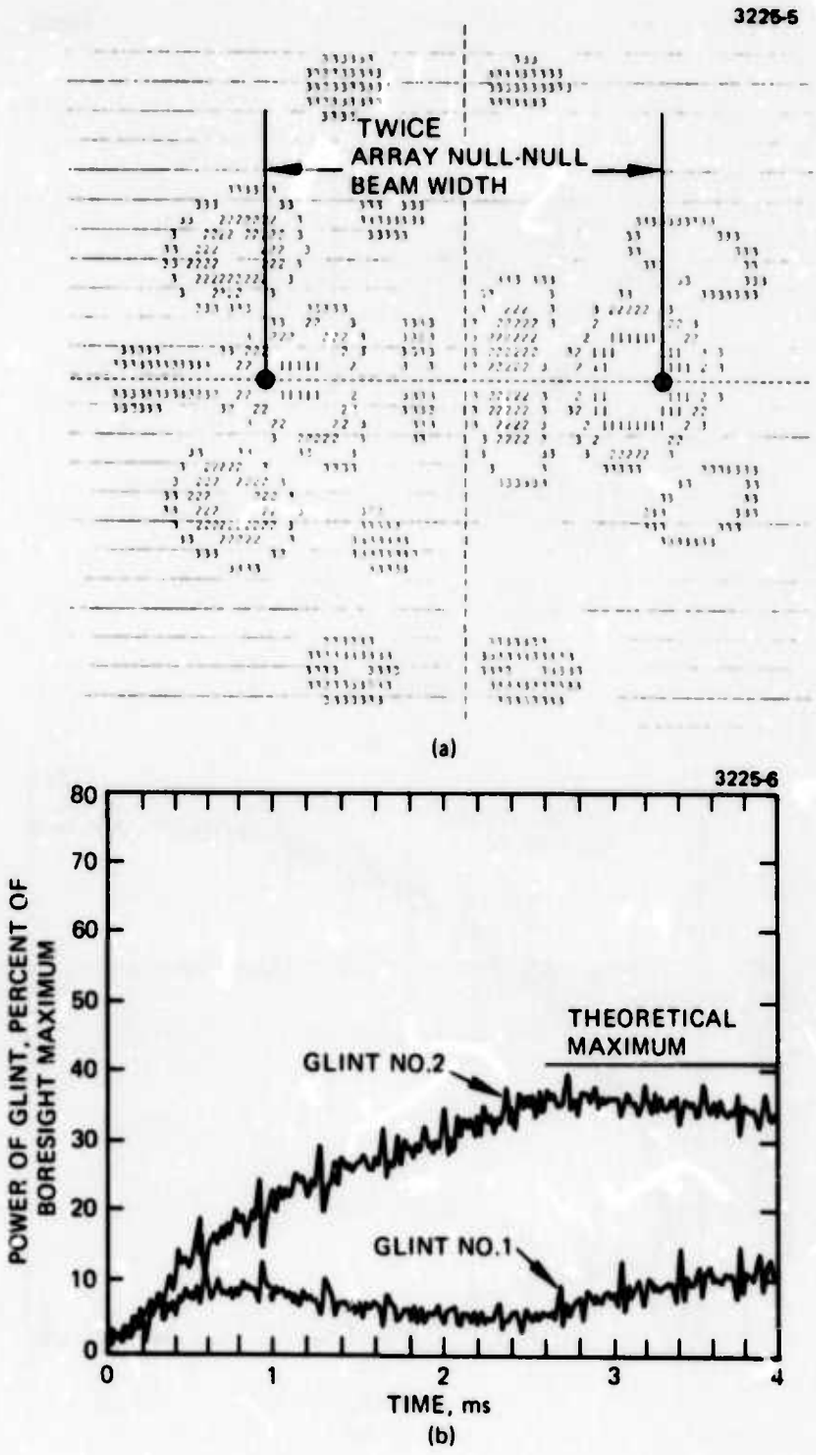

Fig. 4. Convergence run for two eaual glints spaced at twice an array null-null beamwidth. (a) Converged pattern after 4 msec. (b) Time history plot of power on each glint.

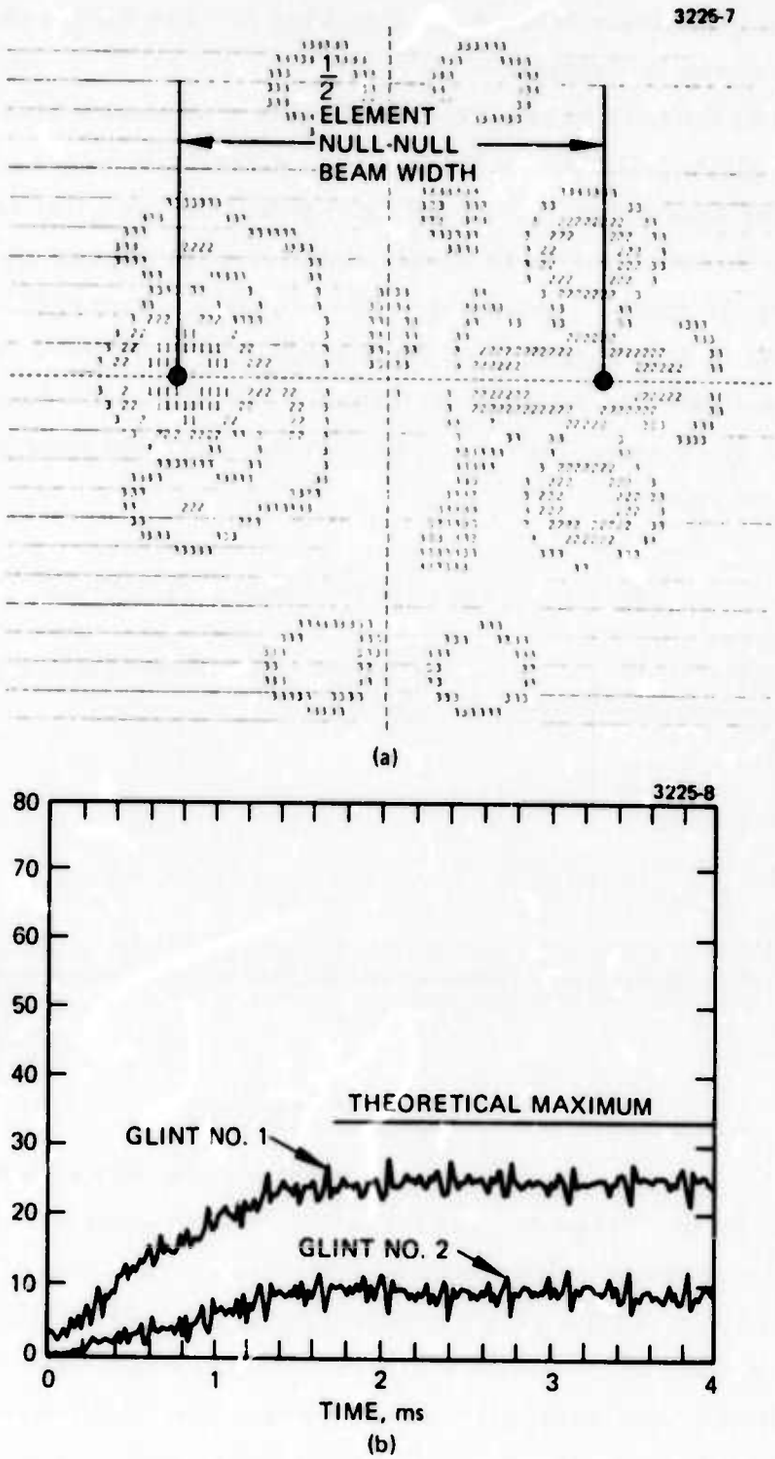

Fig. 5. Convergence run for two equal glints spaced at one-half an element null-null beamwidth. (a) Converged pattern after 4 msec. (b) Time history plot of power on each glint.

increases progressively from Fig. 3 to Fig. 5. The target plane power plot code is shown in Table I.

In each of these cases the COAT system formed a stable beam maximum on one glint. For the cases in Figs. 4 and 5, however, there is some power sharing with about 75% of the total power on one glint and 25% on the other. Note that the system will select either glint depending on the glint locations and the initial conditions. The observed convergence time of 2.0 to 2.5 ms is also longer than for a single glint, or for a multiglint target with a single strong glint (1.0 ms). The important conclusion, however, is that the system does converge on one glint and does not oscillate between the two glints.

Table I. Target Plane Power Plot Code

Digit	dB Down from Boresight Maximum
0	0 to -3
1	-6 to -9
2	-12 to -15
3	-18 to -21

T1116

2. Two Glints of Different Reflectivity

For these tests, two glints were placed as shown in Fig. 6. The reflectivity (backscatter cross-section = σ) of glint No. 1 is varied with respect to the constant reflectivity of glint No. 2. The two glint locations are exactly equivalent, so the glints are distinguished only by their reflectivity.

The results of these tests are indicated in Fig. 7 for two different initial conditions, and with and without noise. The COAT system always converges on the stronger glint if the glint reflectivities differ by more than 30% (σ_2/σ_1 = 1.3 or 1 dB). The convergence time is minimum (roughly 0.8 to 1.0 ms), and the convergence is also complete; there is no splitting of the power between the glints. The weaker glint thus has only the normal sidelobe level power on it. This behavior was observed with different

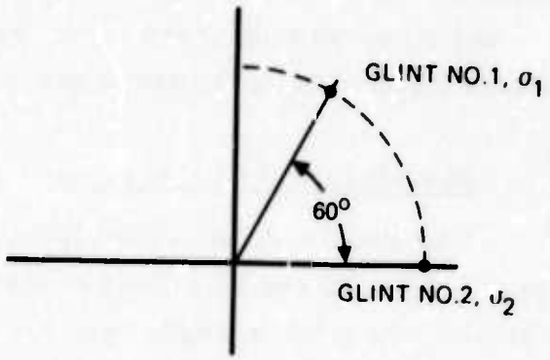

Fig. 6.
Glint configuration for two glint tests. Both glints are one-half of an element null-null beamwidth from the boresight. The glints are also separated by one-half of an element beamwidth.

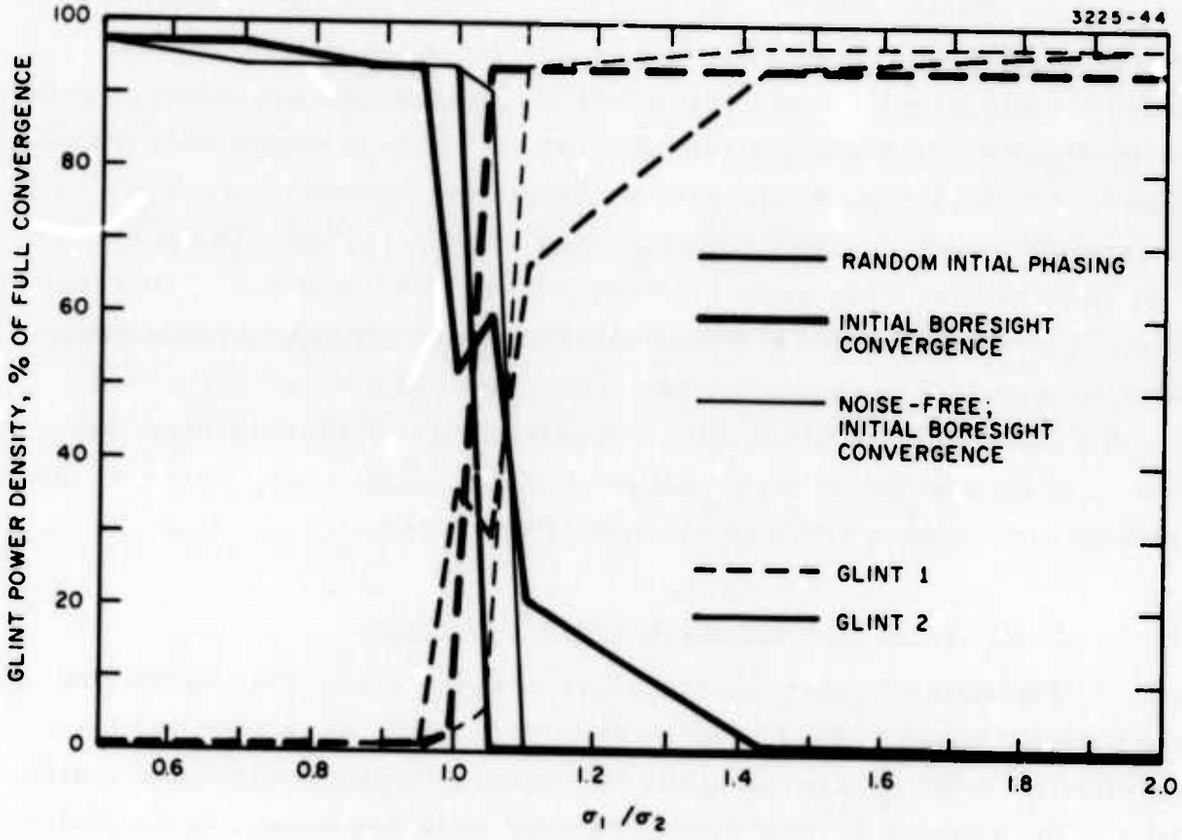

Fig. 7. Final converged power on each of two resolvable glints (configured as in Fig. 6) for three different initial conditions as a function of the ratio of glint reflectivities, σ_1/σ_2.

initial convergence conditions, and with and without noise. If the glints differed in cross-section by less than 30%, the type of behavior described for equal glints was observed: the system always converged on a glint, but not consistently on the same one or on the stronger one.

C. Shearing Glint Convergence

The one-fixed, one-moving case discussed in the third quarterly report[1] (Figs. 10 and 11 of that report) was repeated with the AGC operating. As before, the glint strengths are 3:1 (σ_1 larger) and glint No. 1 is moving at 20 mrad/sec with respect to the transmitter. The results are shown in Figs. 8 and 9. In Fig. 8, the time history plot shows that convergence began on the smaller glint (No. 2), while the larger glint (No. 1) was at the edge of the element pattern. As glint No. 1 moves into the element pattern, power on glint No. 2 decreases as power on the large glint increases. After 3.6 ms the glint power changes in accordance with the variation in the element pattern intensity across the aperture. Note in comparison with the last report that the maximum power achieved is somewhat lower (75% versus 83%) due to the AGC gain reduction at convergence. The power contour plots of Fig. 9 are quite different from those without AGC. At 2 ms, a small beam has formed at the small glint and is beginning to fade away. At 4 ms through 8 ms an excellent convergence has been achieved on the moving glint. It is apparent when comparing Figs. 8 and 9 to Figs. 10 and 11 of the previous report[3] that the AGC has significantly improved the system performance with moving, multiglint targets.

D. Convergence as a Function of Signal-to-Noise

The effects of noise on the COAT system were studied by varying the detector voltage signal to noise ratio (S/N). The simulation calculates an effective noise voltage using the S/N which is proportional to the square root of the detector dc level (shot noise) and adds this voltage to the photodetector voltage. The noise voltage has a gaussian distribution with mean at zero and unit standard deviation.

The simulation was run with different voltage signal-to-noise ratios. Although the simulation is usually run with a S/N ratio of 20, the effect of

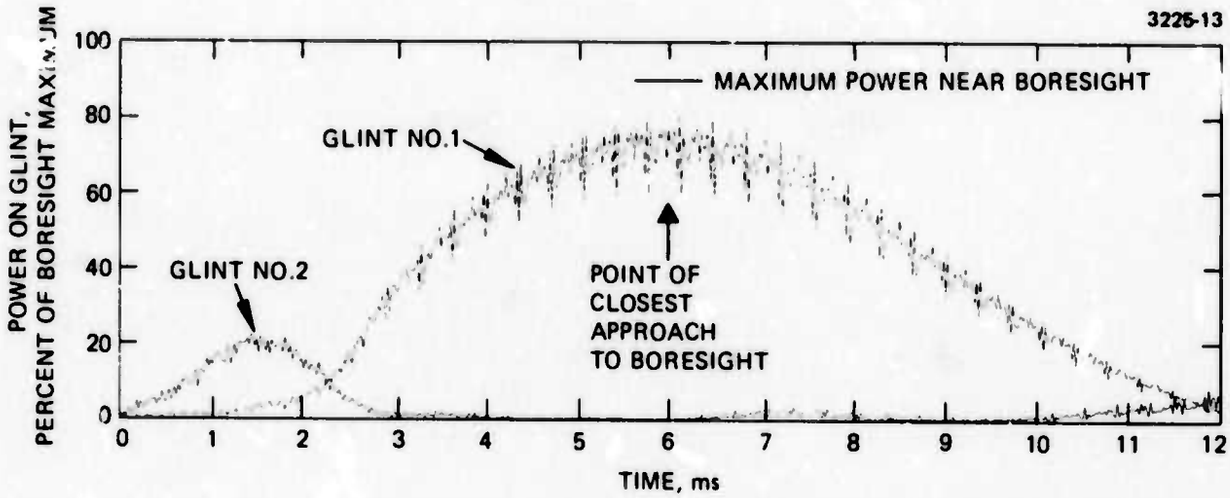

Fig. 8. Power as a function of time on a glint (No. 1) moving near a fixed glint (No. 2). Glint No. 1 is 4.8 dB larger in reflectivity and moves at 20 mrad/sec across the target plane.

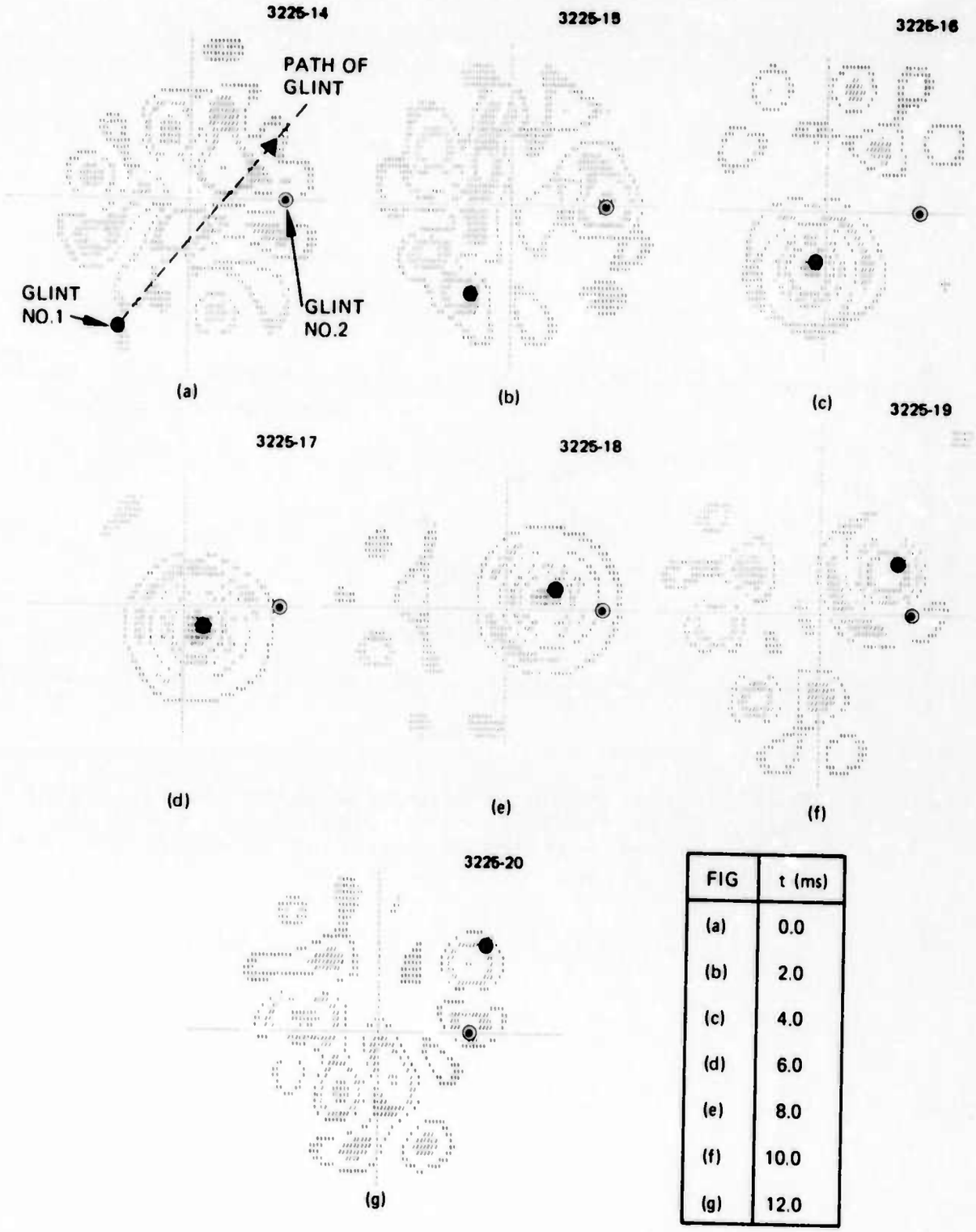

FIG	t (ms)
(a)	0.0
(b)	2.0
(c)	4.0
(d)	6.0
(e)	8.0
(f)	10.0
(g)	12.0

Fig. 9. Power contour plots corresponding to Fig. 8 for one moving and one fixed glint.

noise is most pronounced when the S/N drops below about 5.5. At higher S/N ratios, the main effect is a reduction in the maximum convergence level.[2]

Figure 10 shows glint power time plots for three values of S/N for the two glint geometry shown in Fig. 6 ($\sigma_1/\sigma_2 = 3$). The system stability and maximum convergence level drop very rapidly as the S/N falls below 5.5. For S/N = 3.2, the system never converges on either glint. Noise does not appear to slow down the convergence of the system, but it does cause a reduction and eventually a loss of convergence level.

E. Effect of Receiver Area and Resolution

Several test cases were run to determine the effect of receiver apertures comparable in size to the transmit aperture. A total of six tests were made with a two glint target (Fig. 6). These tests are summarized in Table II, where D_R is the receiver outside diameter, D_T is the transmitter outside diameter, and A_R and A_T are the respective areas.

Table II. Receiver Area Test Cases

Solid Circular Aperture	Annular Aperture (Receiver Inside Diameter = D_T)
A. $D_R = 2\ D_T\ (A_R = 4\ A_T)$	A. $D_R = 2.2\ D_T\ (A_R = 4\ A_T)$
B. $D_R = D_T\ (A_R = A_T)$	B. $D_R = 1.4\ D_T\ (A_R = A_T)$
C. $D_R = 0.32\ D_T\ (A_R = 0.1\ A_T)$	C. $D_R = 1.05\ D_T\ (A_R = 0.1\ A_T)$

T1282

Varying the receiver area is not expected to have any effect with a fixed S/N ratio since the AGC tracks out the variations in signal level. When the maximum receiver diameter (and thus its resolution) falls below that of the transmitter, however, the system's ability to discriminate between multiple glints may be affected. For all of the cases listed in

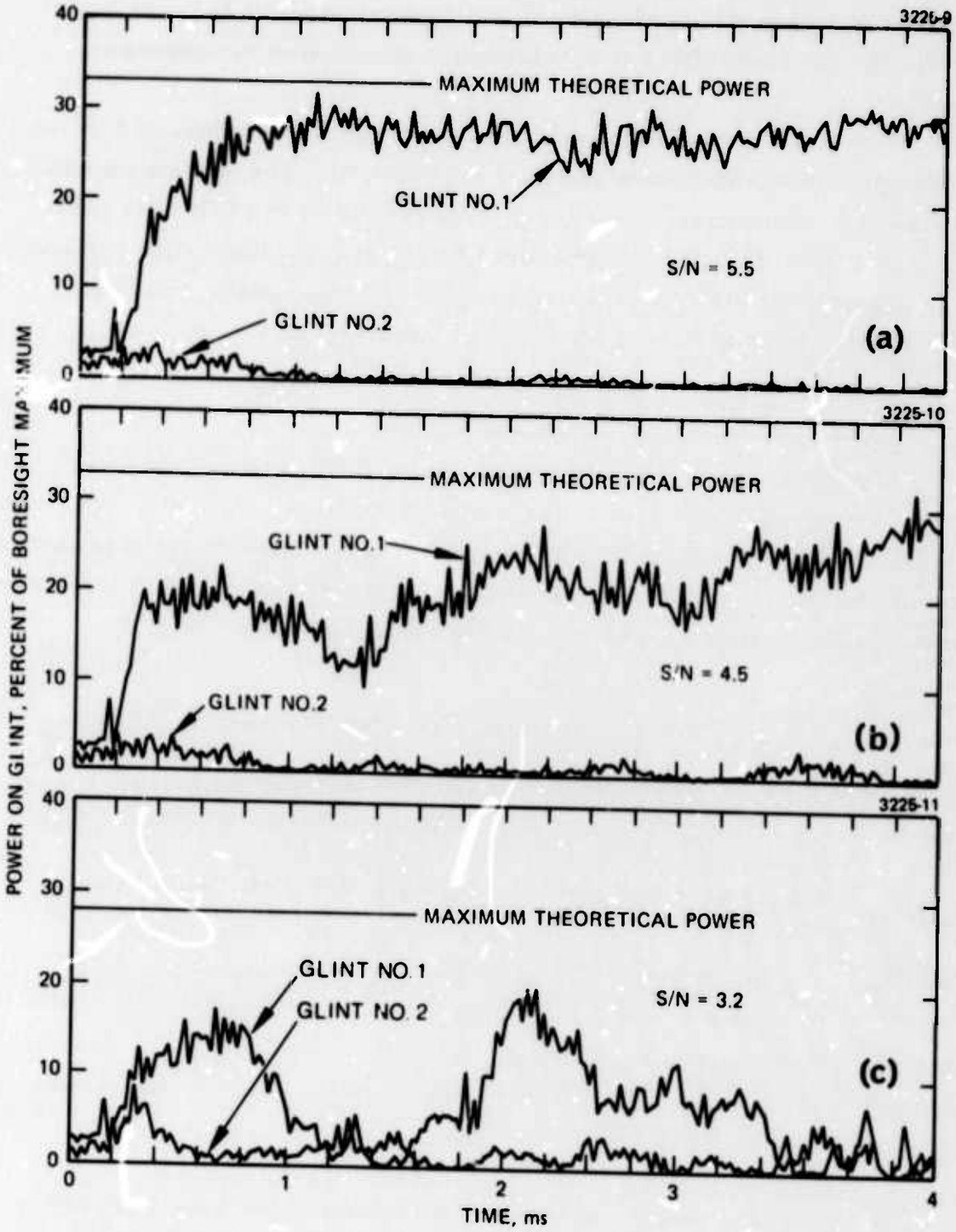

Fig. 10. Convergence sequences for two glints as a function of voltage signal-to-noise ratio (S/N). (a) S/N = 5.5. (b) S/N = 4.5. (c) S/N = 3.2.

Table II, no effects were observed; the system always converged fully on the stronger glint in about 0.8 ms. Similar results were also observed with case C and the annular aperture, but with five glints distributed over the target plane. Further tests are planned to study just how far the receiver resolution can be reduced before the COAT system performance is degraded.

F. Effect of Phase Shifter Hysteresis

Since all piezoelectric devices exhibit hysteresis in their response to an applied voltage, and since PZT drivers are prime candidates for many COAT phase shifter applications, it is important to investigate how such hysteresis affects COAT performance. Although such effects are not observable with the RADC/COAT system, a subroutine has been written for the COAT simulation to study hysteresis effects. The hysteresis loop is represented by

$$D = D_{ST} + \left[(K_B V_{SAT} - D_{ST}) / (\exp(K_H) - 1)\right] X$$

$$\left\{\exp\left[K_H (V - V_{ST}) / (V_{SAT} - V_{ST})\right] - 1\right\} \qquad (1)$$

where

V = applied voltage

D = phase shifter displacement

D_{ST} = displacement at last sign reversal of derivative of applied voltage (loop start displacement)

V_{SAT} = hysteresis loop saturation voltage

K_B = phase shifter constant (meters/volt)

K_H = dimensionless hysteresis constant (loop width parameter)

V_{ST} = voltage at last sign reversal of derivative of applied voltage (loop start voltage).

These quantities are further defined in Fig. 11.

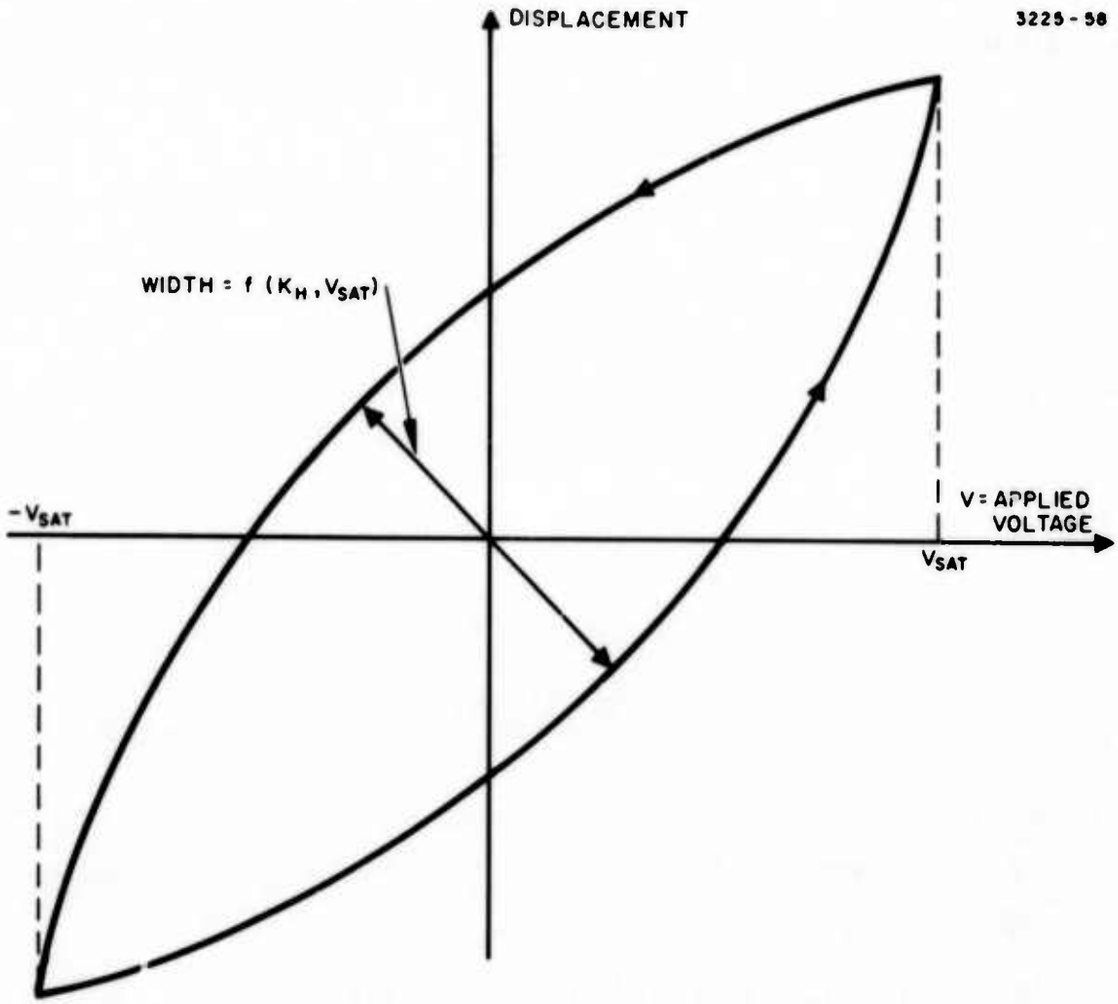

Fig. 11. Definition of hysteresis loop quantities used in phase shifter hysteresis simulation. Loop shown is for a constant amplitude sinusoidal applied voltage with peak amplitude V_{sat}.

Figure 12 presents the results of the test runs. The system convergence time was used as the main performance indicator since the hysteresis had little effect on system stability or final converged level. The results shown in Fig. 12 indicate that hysteresis has very little effect on convergence time until the loop width parameter exceeds 1.2. For larger loop parameters (found only in some magnetic materials), the effect increases monotonically with saturation voltage.

The principle conclusion from these studies is that hysteresis is not likely to present any problems for a COAT servo control system. The non-linear character of hysteresis effects may be important, however, when trying to perform electronic scanning using preprogrammed element offset voltages (as is done in the RADC/COAT system).

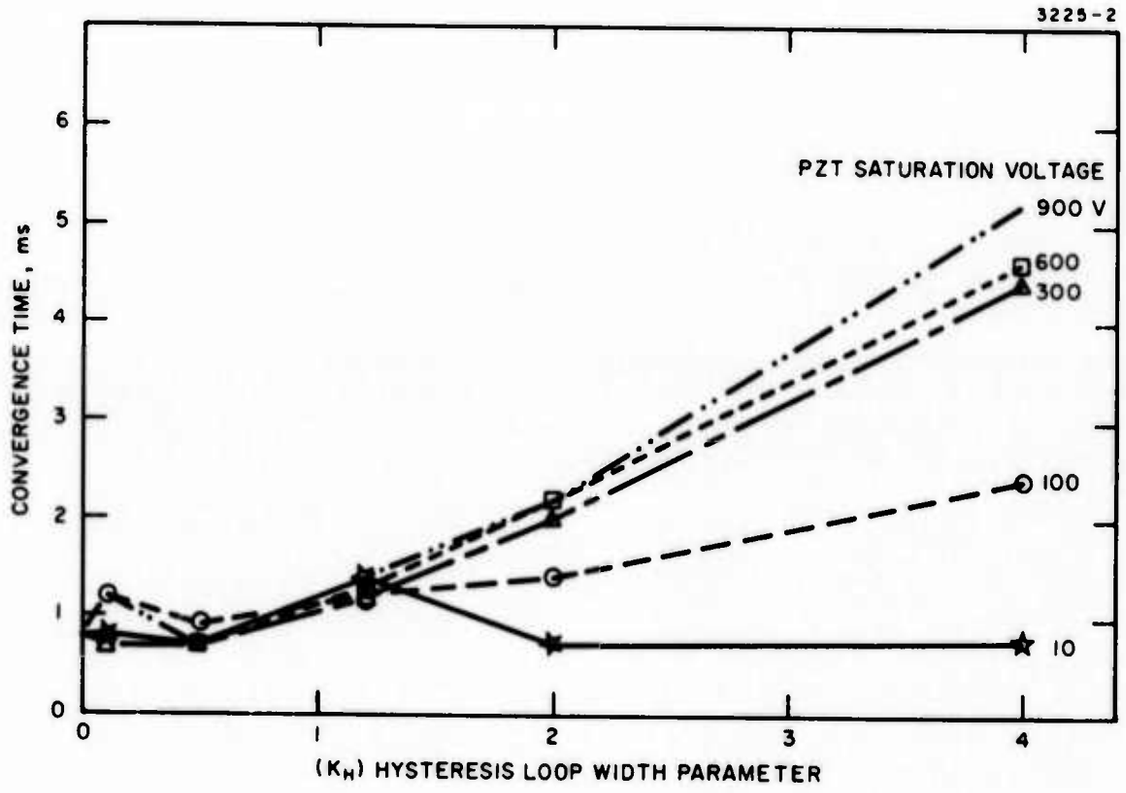

Fig. 12. COAT system convergence time as a function of hysteresis loop parameters.

III. SYSTEM FABRICATION

The 18-element COAT transmitter/receiver system is now complete and tested. The target, along with all of the target analysis equipment, has been assembled and tested. All of the range instrumentation is in place along with the required safety devices. This section discusses the work done during the past quarter on the target analysis equipment and the propagation range. Section IV deals with the transmitter/receiver system calibration. A photograph of the system assembled in the GSG laboratory is shown in Fig. 13; the periscope through which the beam propagates to the roof is shown in the background.

A. Target Analysis Equipment

The target system has been completed and calibrated, and is now mounted in a weathertight enclosure on the range. Figure 14 shows the target rack as it sits inside the enclosure. The optical paths in the target have been described previously.[2]

The laser beam enters the enclosure at a height of one meter above the roof and is turned 90° into a vertical path by a combination of fixed and nutating mirrors. Either the fixed or nutating (when stationary) mirrors may be used to position the beam on a fixed glint target. When the nutating mirror rotates, the optical beam describes an elliptical path with an aspect ratio of two on the glint plane at the top of the rack. From the viewpoint of the COAT transmitter/receiver, this arrangement is equivalent to moving the glint with respect to a stationary beam. The size of the ellipse is controlled by rotating two wedge plates on which the nutating mirror is mounted to change the mirror plane angle with respect to the rotation axis. The size of the ellipse is observed by the TV camera which monitors the target glint positions and the incident beam profile (see Ref. 2). The apparent angular speed of the glint is a function of both the ellipse size and the nutating mirror rotation rate. The rotation rate can be measured either by visual counting or by a tachometer attached to the rotating mirror.

M10314

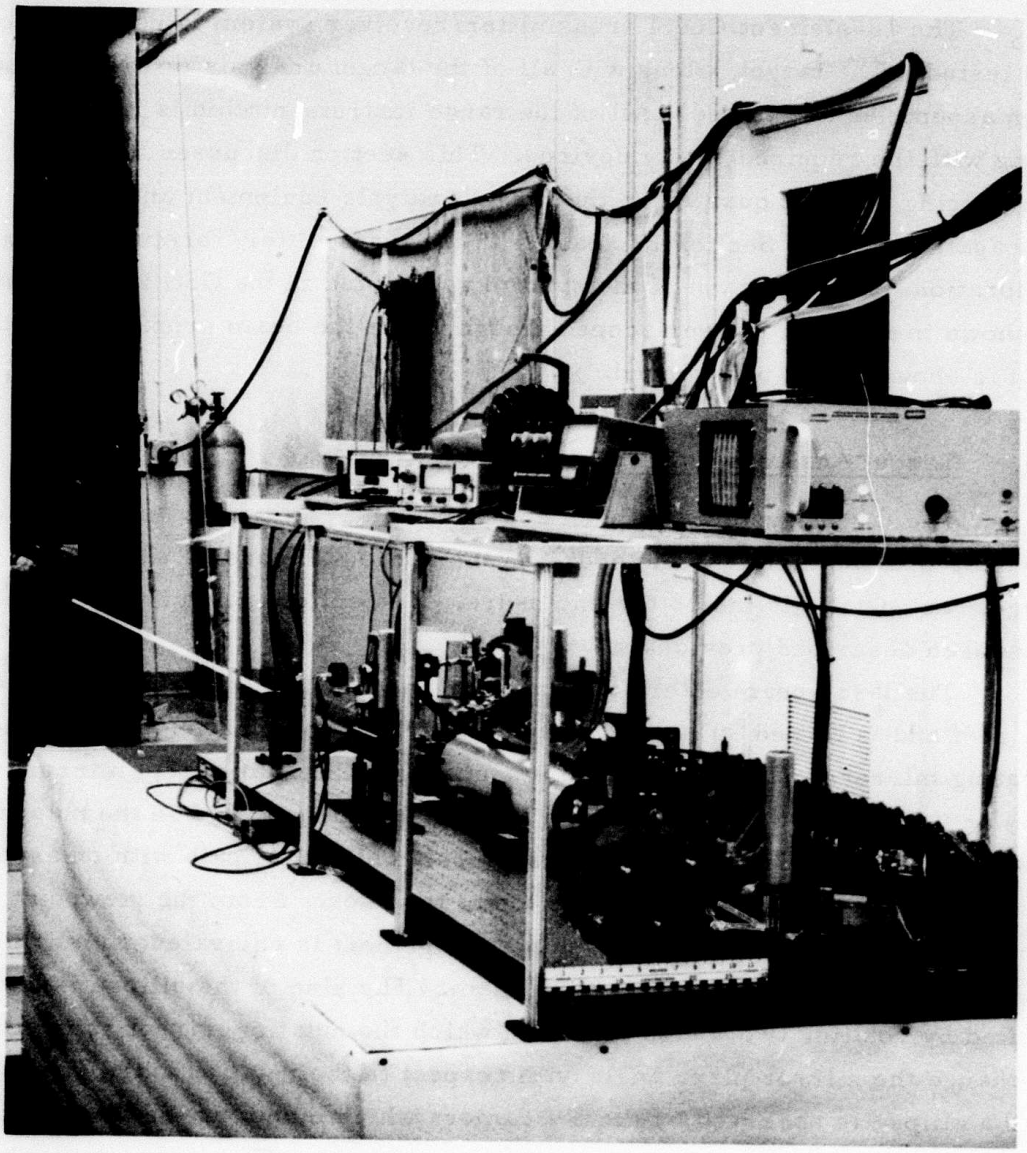

Fig. 13. Photograph of RADC COAT system in the laboratory at the Hughes GSG facility. The periscope which takes the beam to the roof-top propagation range can also be seen.

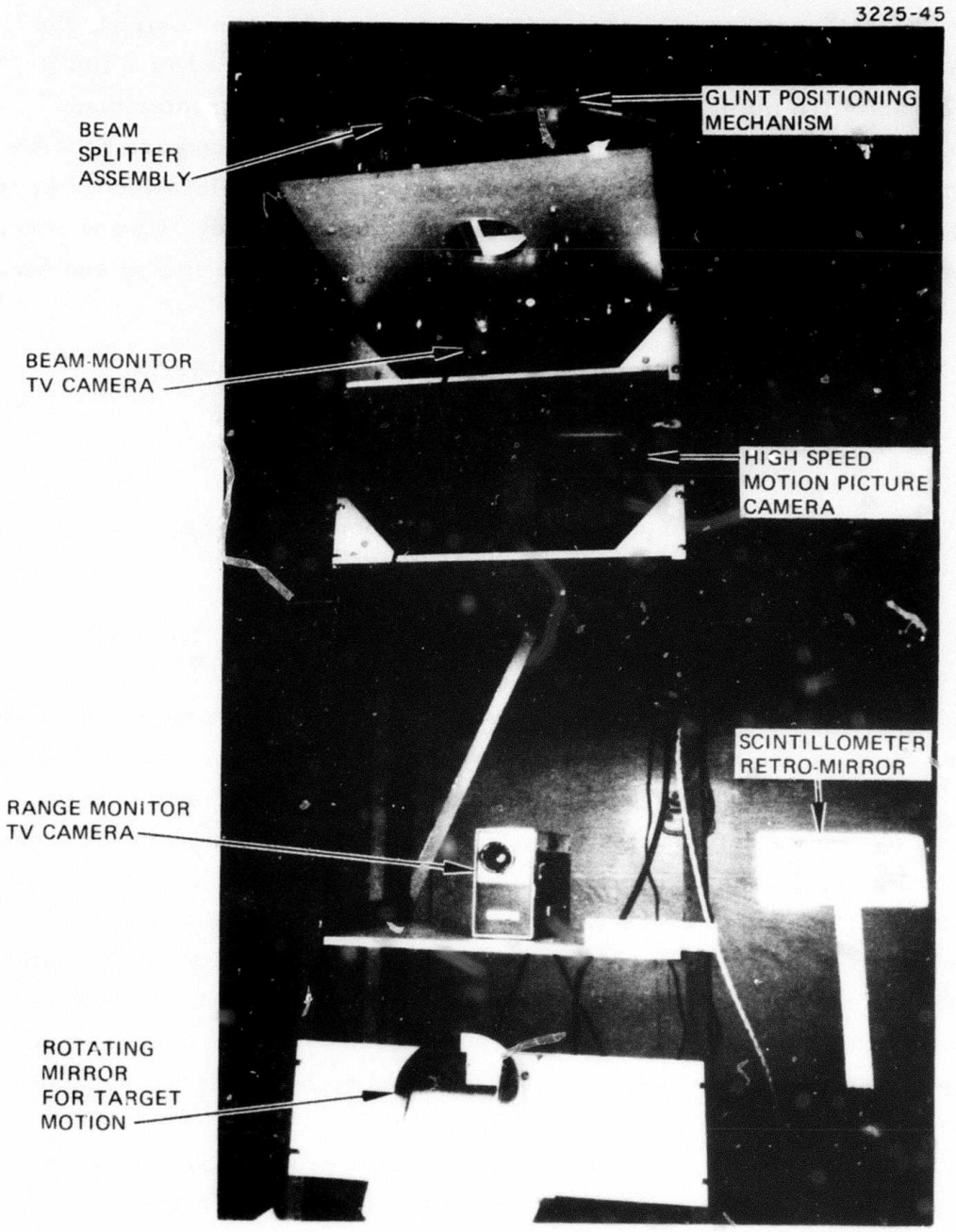

Fig. 14. Photograph of target assembly inside weatherproof housing. The scintillometer retro-mirror used to obtain a 200 m path length can also be seen.

A high speed movie camera is used to record, when desired, the same image as seen by the TV camera. The movie camera has a 100 ft film capacity (16 mm), and can record 1.5 sec of data at greater than 2000 frames per second. Frame rates up to 5000 per second are possible with this camera. Because the camera requies some acceleration time, it must be started before the start of the event to be recorded. This is accomplished by controls supplied with the camera which provide timing and start signals for the event. A typical operating sequence is:

1. Start camera (by remote push button in laboratory).
2. Camera control provides a contact closure in laboratory after 500 ms when frame rate has reached 2000/sec.
3. Contact closure closes control loop on COAT system to demonstrate convergence and beam profile for 1.5 sec.
4. Film runs out and camera control shuts off camera at 2.0 sec.

Event timing is facilitated by timing marks which are produced on the edge of the film by a strobe light energized by an external square wave generator.

Initial tests of the target equipment using the COAT system have uncovered several deficiencies in the TV camera which monitors the target and the incoming beam. The camera has no overrides on its automatic gain control (AGC) or automatic sensitivity control (ASC) and so cannot be used for taking quantitative data. The unit also has poor linearity and the synch signals are not adequate for use with the color quantizer. We have also found that the camera dark current increases substantially as the target enclosure heats up. The dark current becomes so large that the dynamic range of the quantizer is nearly halved.

We have resolved all but the dark current problem by purchasing a high quality camera and lens assembly from Interpretation Systems Inc., the manufacturer of the color quantizer. The new camera has better than 3% amplitude linearity over a 23 dB intensity range, and 3% uniform response across the face of the vidicon. The unit also has manual AGC and ASC and is designed for use with the VP-8 image analyzer (color quantizer). The temperature and dark current problem will still be present, however, so

we are installing cooling equipment to maintain the camera at or below $75^{\circ}F$.

Figure 15 shows the monitoring and recording equipment for the target. The output of the 18-element phasor matrix is displayed on the TV target monitors. An oscilloscope is used as an xyz display for observing the target monitor outputs in profile or in pseudo-3D isometric display. The target black-and-white monitor shows the input to the quantizer, and the target color monitor presents the same video in color, with each color representing a different intensity level. A cassette video tape recorder is available for permanent recording of desired data. The second black and white monitor is driven by a camera placed at the range target which looks from the target down the range to the periscope.

The image analyzer (color quantizer) is proving to be a very useful instrument for recording system performance both qualitatively and quantitatively. Some preliminary pictures of the converged and unconverged beams are shown in Fig. 16. The black and white pictures were made from Polaroid color prints so the full impact of the display is not apparent. The color bands at the bottom of the pictures indicate the relative size of the intensity bands corresponding to each color. These bands are variable and can be calibrated so that each color represents any desired range of intensity.

B. Propagation Range

1. Range Instrumentation

All of the necessary cabling for the target monitoring instruments has been completed (cabling for cameras, glint power detectors, power controls, and atmospheric instruments). The required safety devices which include a rope fence, warning signs, and a flashing red light are in place and operating. In addition to a 24-hour recording instrument for temperature, pressure and humidity, we now have a wind direction and velocity meter with a remote indicator in the lab.

We have been using the output of a differential microthermometer as the principal measure of C_n so far. The scintillometer and MTF monitor have not been used because of problems in maintaining a stable alignment of

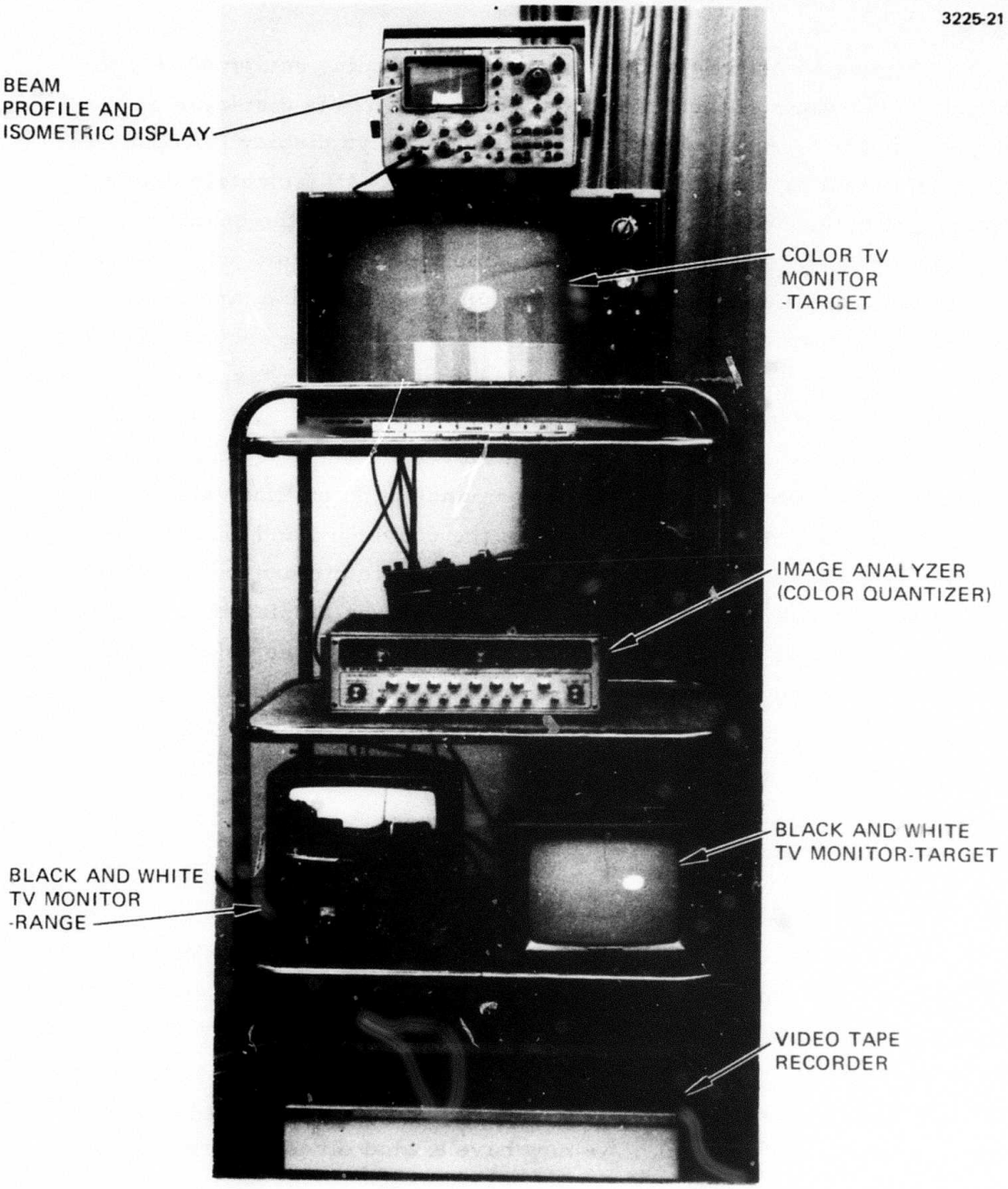

Fig. 15. Target monitoring and data recording equipment rack.

M10315

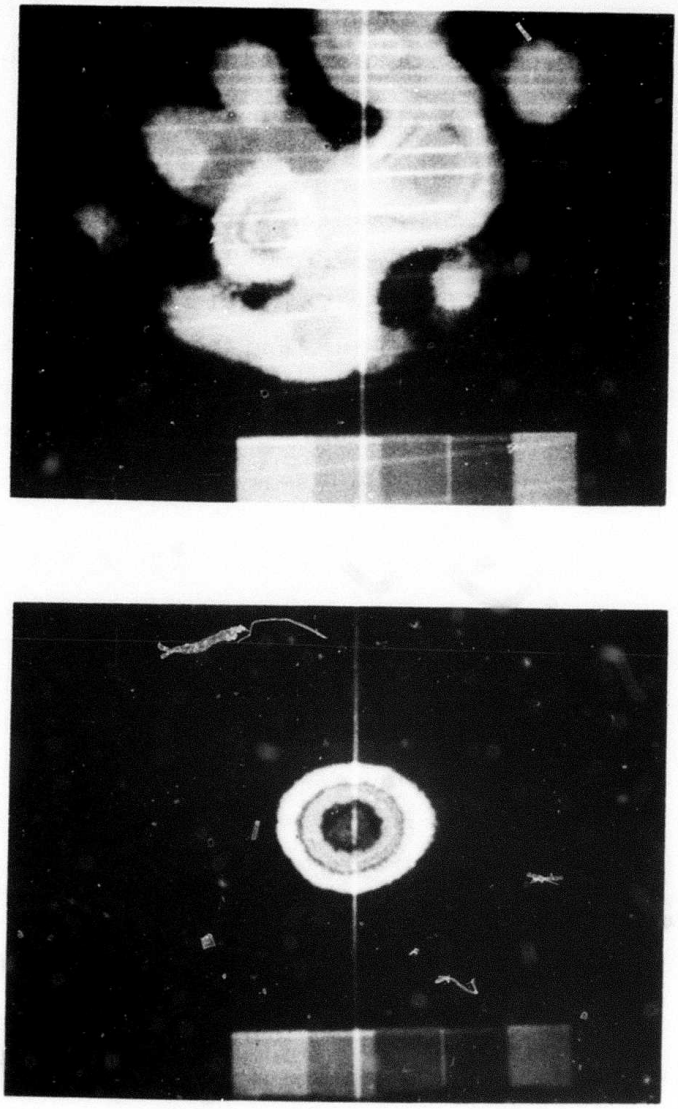

Fig. 16. Black-and-white photographs of color monitor display of image analyzer (color quantizer) output. (a) Unconverged 18-element far-field pattern (COAT off). (b) COAT on, converged beam pattern.

the required optical paths. We are continuing to work on solving the problems with these instruments, and expect to be using all three on a daily basis within the next few weeks.

2. Range Construction

The periscope modifications which were in progress during the last reporting period are now completed. Physically, the periscope is 30 in. in diameter and 30 ft in length. The first 24 ft from the base to the roofline is in an air-conditioned building, and the remaining 6 ft extends above the roofline and is exposed to external ambient conditions. Since the top and bottom of the periscope are exposed to different environments, care was taken to seal any openings to minimize convection air currents within the tube.

Microthermometer measurements were made to estimate the turbulence levels in various portions of the periscope range optical path. Four measuring locations were used: in the bottom of the periscope, in the top of the periscope, and the normal mid-range location. The microthermometer was placed in each of these locations and data taken for a 24-hour period. The periscope was sealed as tightly as possible as it is in normal operation. The data indicate that the turbulence in the laboratory and the periscope is small relative to the rooftop mid-range turbulence. Initially, however, the turbulence in the top of the periscope was larger than desired. Household insulation material was wrapped around the top of the periscope with the metallic side out to reduce the effects of heat loading by the sun. Turbulence levels measured after the insulation was installed were comparable to the low values in the laboratory and at the bottom of the periscope. The results of the measurements are summarized in Table III.

The data in Table III indicate that the laboratory path (about 6 m) and the periscope path (10 m) will contribute negligible turbulence fluctuations compared to the 92 m rooftop path. Since the rooftop range is very uniform, the microthermometer should give values for C_n which are an accurate measure of the turbulence over the entire path. This should be true even for low turbulence levels ($C_n^2 \sim 2 \times 10^{-16}$ $cm^{-2/3}$) since the laboratory and periscope paths are so short compared to the rooftop path.

The scintillometer and MTF monitor should, however, provide a check on this conclusion.

Table III. Microthermometer Measurements of Turbulence Levels at Various Locations

Location	Range of C_n^2 ($cm^{-2/3}$) Over 24 Hours
Laboratory	6×10^{-17} (instrument noise level) to 2×10^{-16}
Inside bottom periscope; periscope sealed shut.	6×10^{-17}; no variation
Inside top of periscope; no insulation.	6×10^{-17} to 4×10^{-16}
Inside top of periscope; insulation installed.	6×10^{-17}; no variation
Mid-range	1×10^{-16} to 6×10^{-15}

T1283

IV. LABORATORY MEASUREMENTS: SYSTEM CALIBRATION

A. 18-Element Array Far-Field Patterns

1. Element Patterns

Figure 17 shows the far field pattern for each element of the 18-element array. The patterns were photographed with the same exposure times using the arrangement shown in Fig. 18. Small variations in the observed patterns are caused either by the different element shapes or orientations, or by small mirror distortions which degrade the pattern from its undistorted form. Table IV indicates the relative peak intensity in the far field accurate to about ±10% measured on each element using a pinhole detector on the common element boresight axis. The power is quite uniform across the aperture. The collimating lens used for these measurements provides a $1/e^2$ beam radius of 13 mm so that the intensity is down to 0.52 (on-axis intensity = 1.0) at the 7.4 mm outer radius of the array pattern, 0.88 at the intermediate radius, and only 0.97 at the inner radius. The values given in Table IV are consistent with these numbers. Unfortunately, only about 20 mW maximum is available at the output of the phasor matrix. Reducing the beam size at the input to the phasor matrix to 7.5 mm radius will increase the output to about 30 mW at the expense of less uniformity in power per element. If still higher powers are desired, it will be necessary to put antireflection coating on many of the optical surfaces in the system.

2. Array Patterns

The far field pattern of the COAT-formed 18-element array is shown in Fig. 19. The pictures shown in Fig. 19(a) are to the same scale as the element patterns shown in Fig. 17. Comparing the null-to-null beamwidths in Figs. 17 and 19 gives

$$\frac{\text{(Array beamwidth)}}{\text{(Element beamwidth)}} = 4.7 \pm 0.3$$

compared to a theoretical maximum of 5.0.

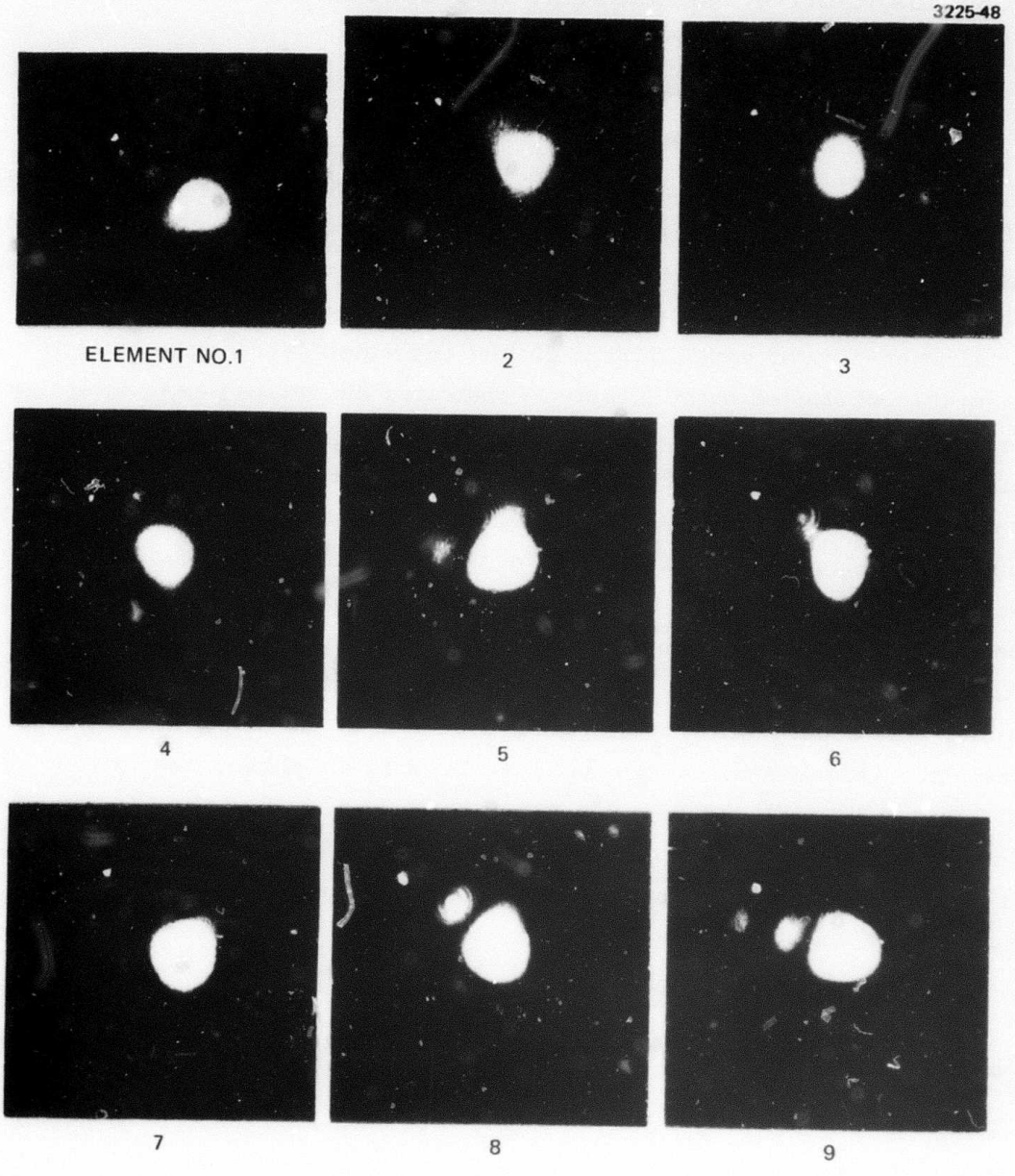

(a) Elements 1-9

Fig. 17. Far-field element patterns for each of the 18 system elements in the 0-6-12 array. See Fig. 18 for shape of elements and their positions in the array near-field.

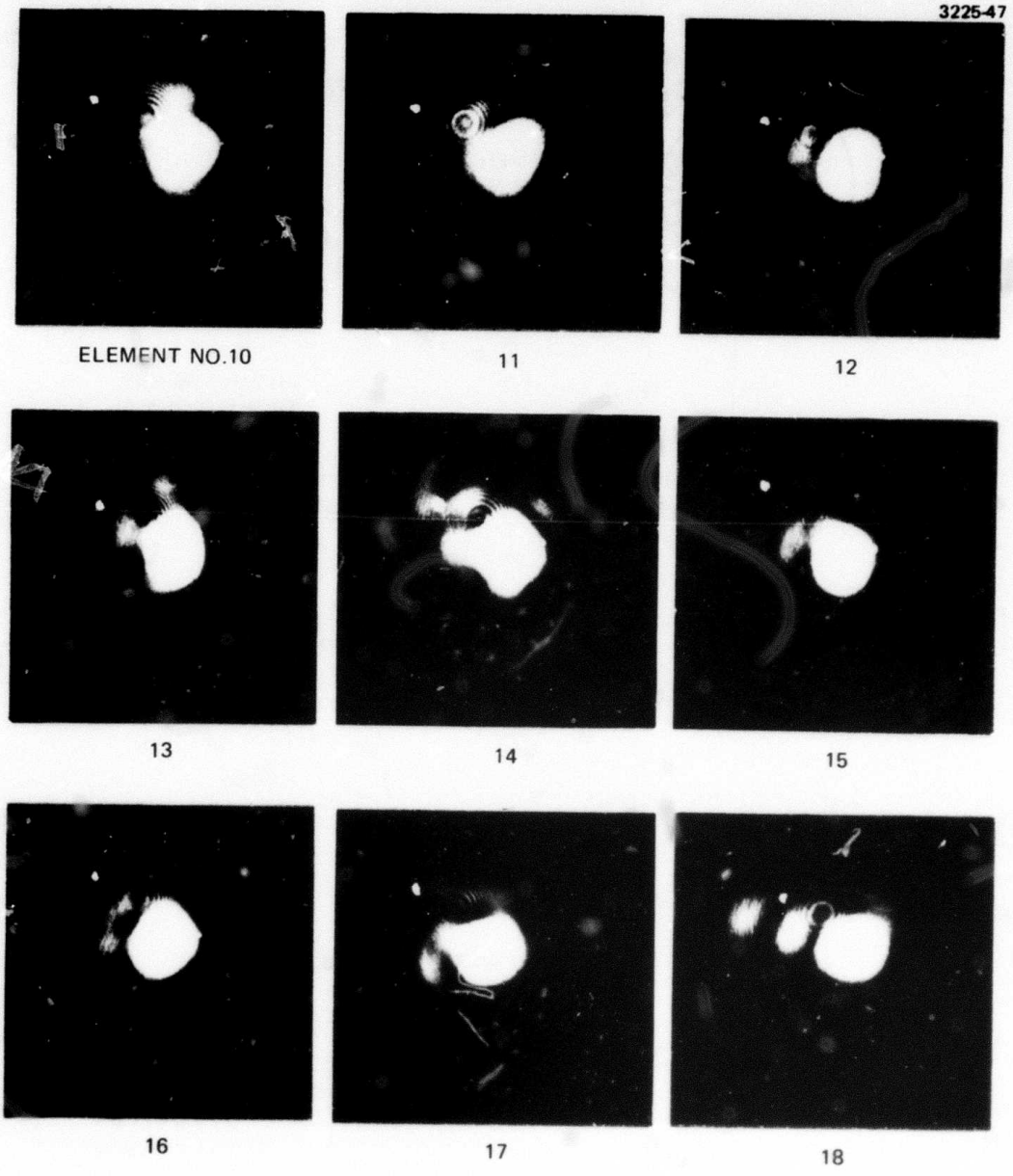

(b) Elements 10-18

Fig. 17. (Continued).

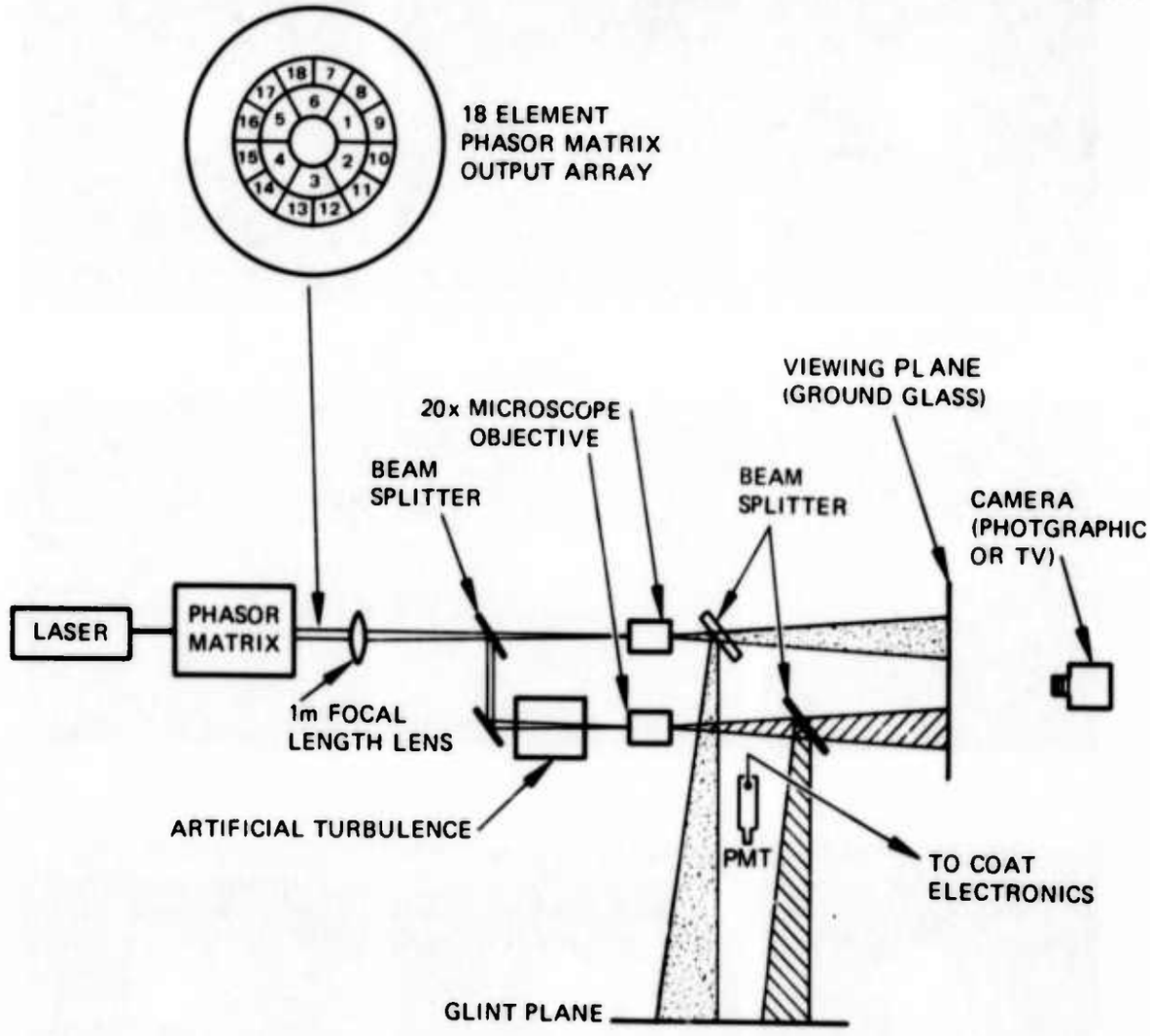

Fig. 18. Multiple path arrangement for laboratory measurements. Two identical paths are provided by the beam splitters, the 1m focal length lens, and the two 20x objectives. Artificial turbulence is introduced into only one path.

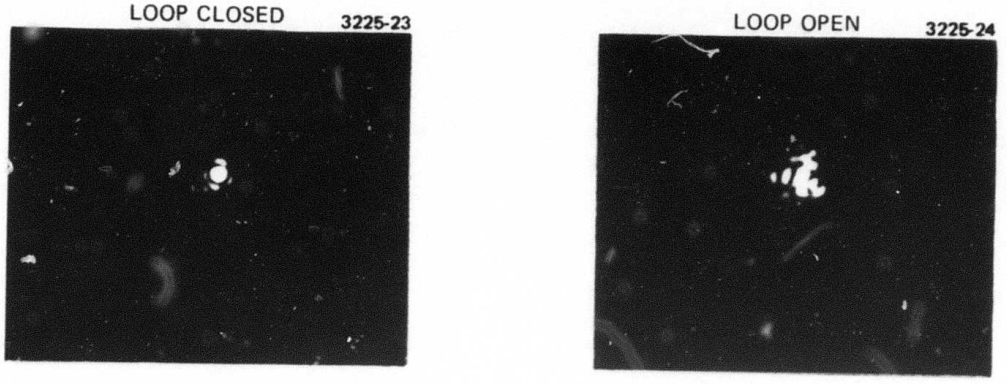

(a) DIRECT PHOTOGRAPH

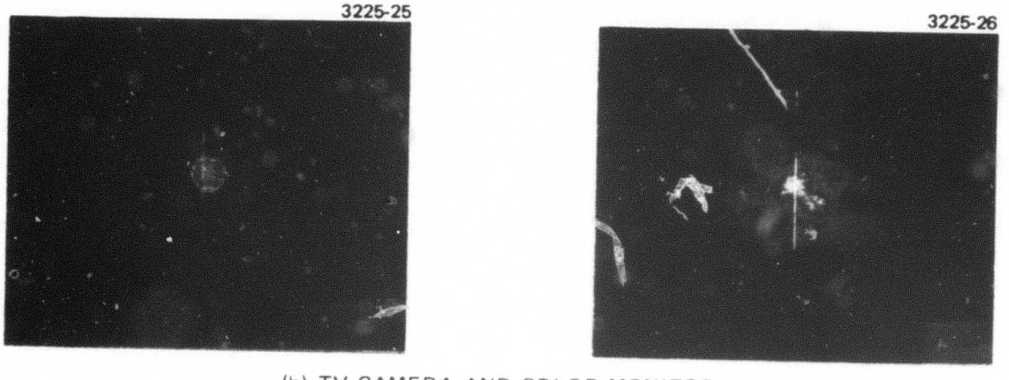

(b) TV CAMERA AND COLOR MONITOR

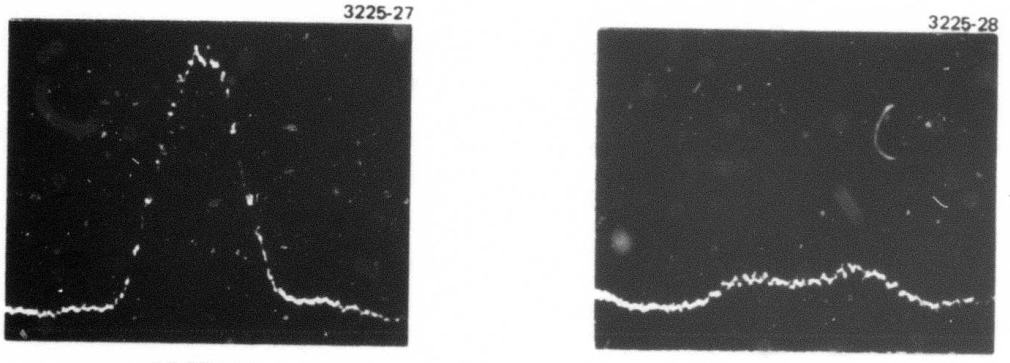

COAT ON

COAT OFF

(c) LINE SCAN WITH COLOR QUANTIZER

Fig. 19. Array far-field patterns in the laboratory for COAT on (loop closed, left-hand photos) and COAT off (loop open, right-hand photos). (a) Direct photograph of beam. (b) Color TV monitor display of (a). (c) Line scan along vertical line shown in (b).

Table IV. Relative Peak Intensity per Element in an 18-Element Aperture

Elementary Number	Peak Intensity	Elementary Number	Peak Intensity	Elementary Number	Peak Intensity
1	0.77	7	0.89	13	0.79
2	0.82	8	1.0	14	0.55
3	0.84	9	0.72	15	0.82
4	0.98	10	0.70	16	0.88
5	0.77	11	0.67	17	0.85
6	0.90	12	0.86	18	0.95

T1284

The photographs in Fig. 19(b) were made directly from the color monitor using black and white Polaroid film. The bands at the bottom of the pictures indicate the various intensity levels, the lowest being the band at the left of the picture.

The curves in Fig. 19(c) are intensity profiles through the vertical scan line shown as a white line in Fig. 19(b). This display is produced by a highlighted portion of the isometric display produced by the image analyzer and viewed on an oscilloscope (see Fig. 15). The effect of closing the COAT control loop is quite dramatic, but opening and closing the loop is really not a fair measure of COAT performance since the loop open state is some randomly phased condition. A better test is to start with a diffraction-limited beam (perfectly phase the COAT array); put this beam through some kind of distortions such as turbulence, and observe the resultant beam both with and without COAT corrections. The experimental arrangement shown in Fig. 18 is designed to provide this type of comparison, and results are discussed in Section IV-C and Section V. As a final example, Fig. 20 shows a computer-generated plot of a beam scanned off boresight compared to a similar experimental pattern. Note the high degree of similarity between the two figures. The experimental pattern

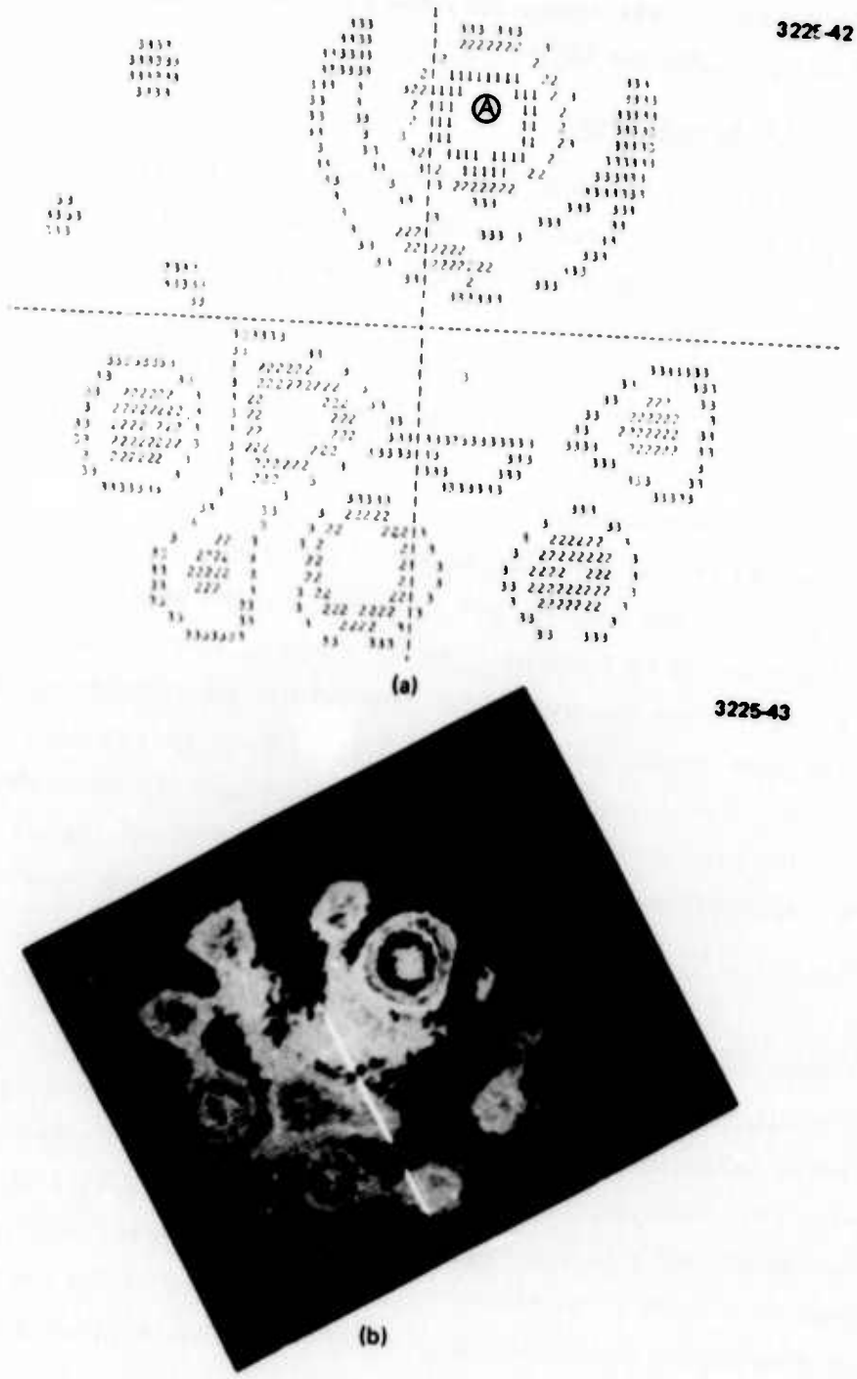

Fig. 20. Comparison of computer-generated power plot, (a), with color monitor display of system-formed beam, (b). The glint has been placed off boresight by one-fourth an element null-null beamwidth (glint is at "A").

has been rotated because the symmetry axes of the computer array and the experimental array differ by 30°.

3. Tracking Modes

There are three principle modes in which the COAT system can operate: glint tracking, edge tracking (similar to glint tracking), and black hole tracking. An example of glint tracking is shown in Fig. 21. This is the usual mode of operation in which the COAT system forms the beam on the brightest glint in the array field of view. The beam to the left of the "realistic target" in Fig. 21 is identical to the beam on the target; a beam splitter was used to produce this beam since the target tends to obscure the details of the beam pattern.

If the target is a bright diffuse reflector with no glint points against a darker background, the COAT system will form the beam on boundary between the light and dark regions. An example of this tracking mode is shown in Fig. 22. When the system is phased for glint tracking, the beam will be formed just inside the lighter (higher reflecting) region.

By simply reversing the phase of the feedback signal in the COAT control loop, the system will try to minimize the received signal by forming the beam on a nonreflecting part of the target. This "black hole" tracking mode is illustrated in Fig. 23.

B. Convergence Performance

One change was made in the COAT servo loop when the system was moved to the propagation range at Hughes GSG facility in Fullerton. The dc gain following the multiplier in each channel was lowered by a factor of 10 to reduce problems with dc offset drift in the multipliers. The reduction in loop gain was then to be compensated by ac gain ahead of the multipliers. The change was fine in principle, but evidently not so in practice. The noise levels are high enough that the clipper preceding the multipliers prevents achieving sufficient ac gain to offset the dc gain reduction. The net result was to increase the convergence time from about 1 ms up to 2 or 3 ms. This is not a fundamental limitation, but rather a result of our choices of electronic parameters. If time permits we will make some modifications to

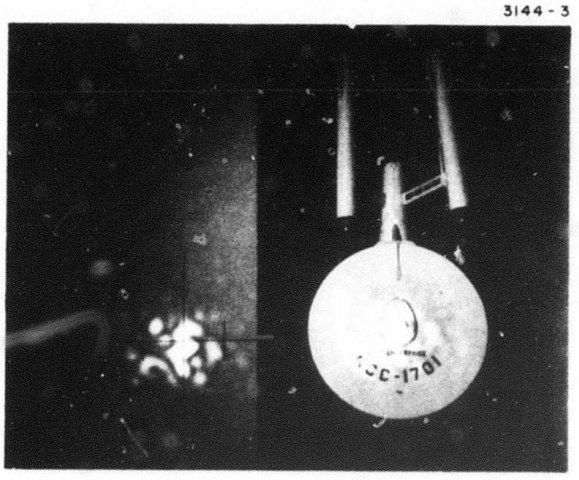

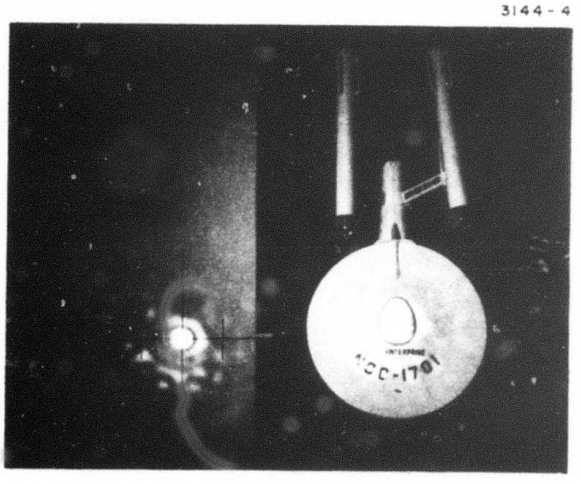

Fig. 21. Example of COAT operation in glint-tracking mode.

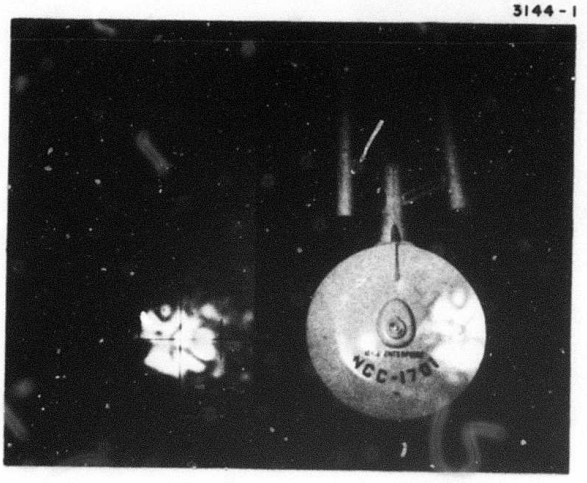

COAT INOPERATIVE

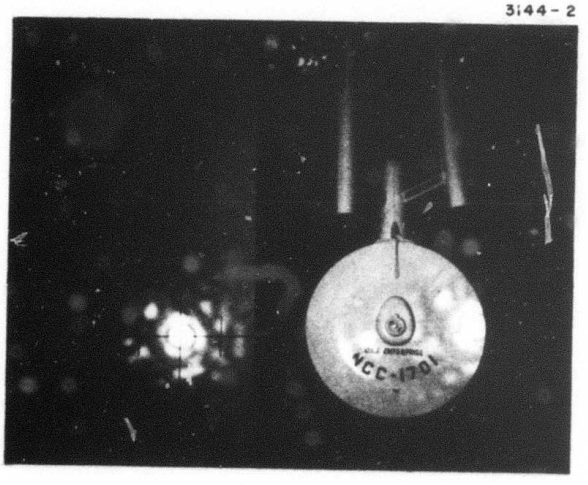

COAT IN EDGE TRACKING MODE

Fig. 22. Example of COAT operation in edge-tracking mode.

GLINT TRACKING MODE:
BEAM FORMS ON A GLINT
(CENTRAL CANOPY AREA)

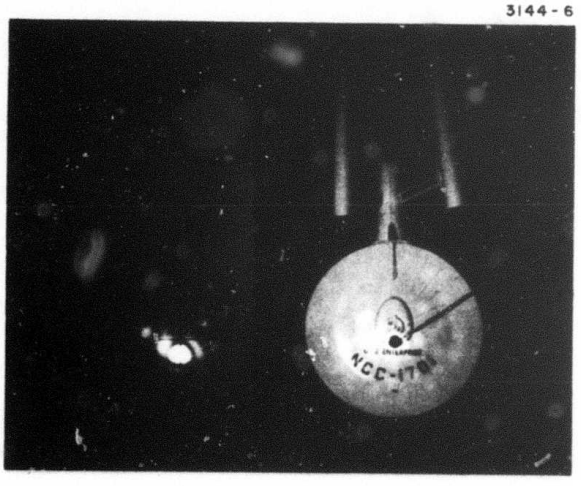

ELECTRONIC SWITCHING TO
BLACK HOLE TRACKING
MODE (BLACK HOLE JUST
BELOW GLINT)

Fig. 23. Example of COAT operation in black-hole tracking mode.

both the ac and dc portions of the control system to increase the convergence time.

1. Effect of Gain on Convergence Time

Previous simulation studies[2] have indicated that the product of gain and convergence time is approximately constant. The effect of gain on convergence time was measured with the RADC/COAT system in the laboratory with no turbulence, and before the reduction of dc gain discussed above. A linear 8-element array was used. The results presented in Fig. 24 agree well with the constant product relationship. The data points in Fig. 24 indicate the average of a number of runs, and the vertical bars indicate the range of observed values for τ_c.

2. AGC Performance

The previous report[1] presented some preliminary comparisons of system performance without AGC and with two different types of AGC. These studies have been continued with representative results shown in Fig. 25. The data show the photomultiplier signal and the power on the glint as a function of time. The zero time point occurs when the control loop is closed. In each case, the loop voltage gain is optimized for minimum convergence time with stable convergence. These data were taken after the system was moved to Fullerton so the effect of the lower dc gain is present. No additional amplifiers are used with the i. f. -AGC, but two amplifiers — one dc coupled, one ac coupled — are used with the divider-AGC and for the no-AGC data.

Contrary to the computer simulation results, the i. f. -AGC and the divider-AGC give almost identical performance. The convergence time is 2 to 3 ms with less than 1 ms delay (in most cases). As has been observed previously, both the delay from the loop closing to the start of convergence and the convergence time vary by about a factor of 2 from run to run. Figure 25(c) shows an unusual convergence cycle where the array began to converge, then "deconverged" and finally started again, achieving convergence in 2 ms after the second start. This type of behavior is observed occasionally, but the cause of it is not understood.

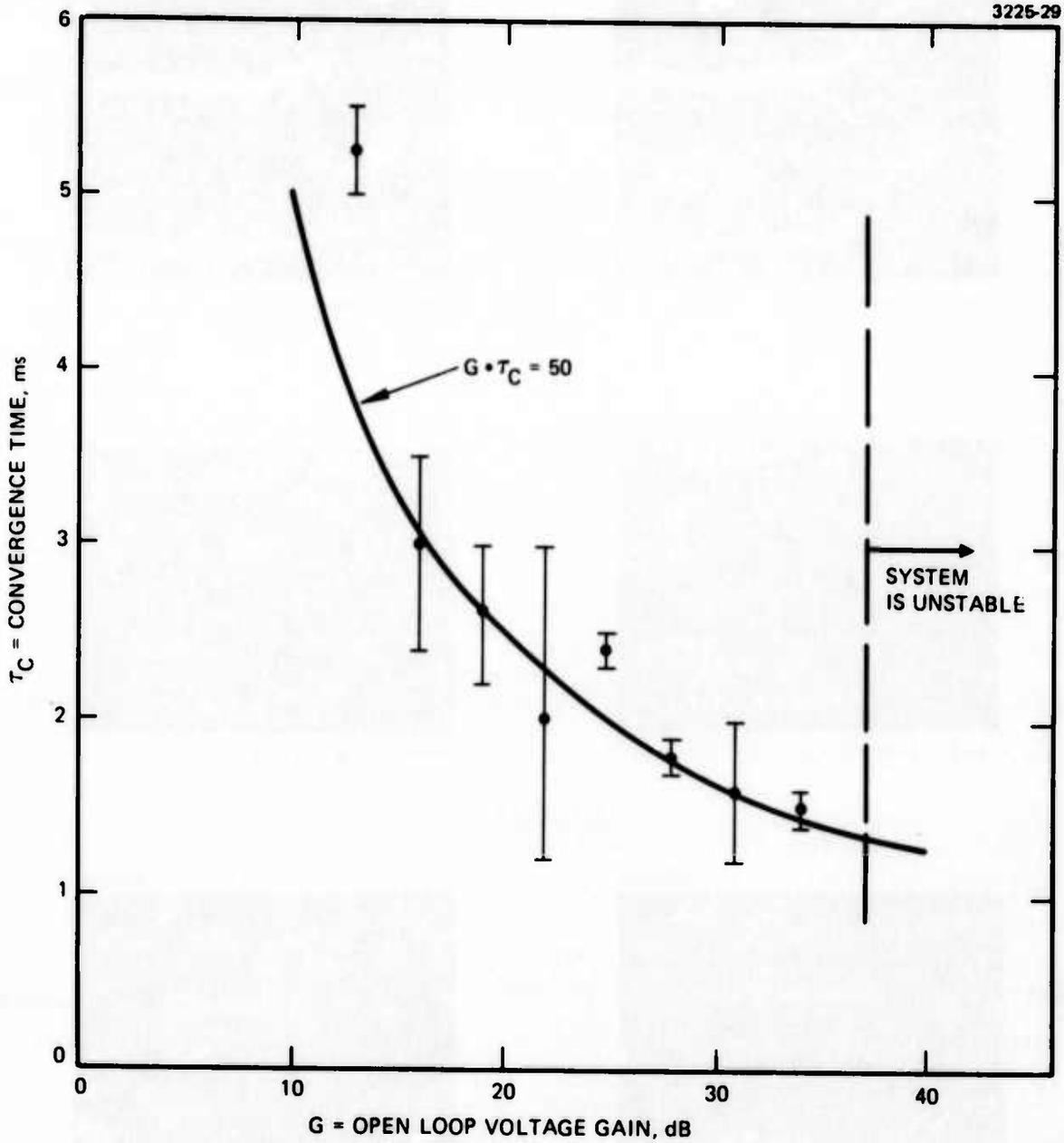

Fig. 24. Experimental data showing the effect of open-loop gain on convergence time. The $G \cdot \tau_C = 50$ curve is a best-fit to the data; the constant product theoretical curve is also predicted by computer simulation.

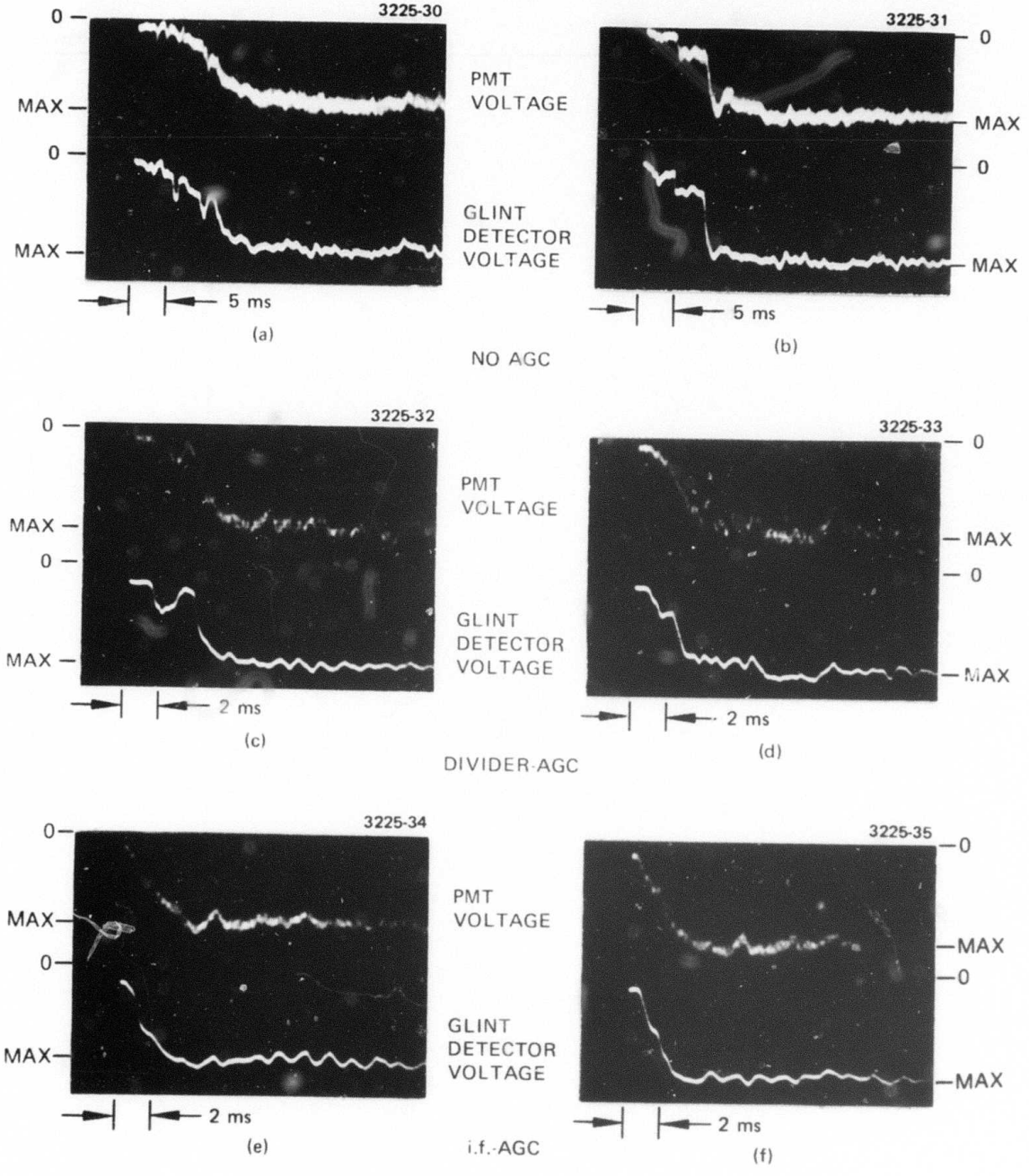

Fig. 25. Comparison of convergence time as a function of AGC. performance. (a) and (b) No AGC, loop gain maximized with stable convergence. (c) and (d) Divider-AGC. (e) and (f) i.f.-AGC. Note the different time scales.

The disagreement between the computer simulation results and the data shown in Fig. 25 is probably a result of our inability to accurately model the dynamic characteristics of the i. f. -AGC. For all future tests, unless otherwise noted, the i. f. -AGC will be used since it seems to give slightly better performance.

3. Glint Discrimination

The ability of the COAT system to discriminate between two nearly equal glints has been investigated using a linear 1 x 8 array. Two equal lengths of 1-mm wide scotchlite were placed equal distances on opposite sides of the boresight axis. Each glint was separately unresolvable but the glint spacing was resolvable (about 1. 5 of an element beam width or 8/5 of an array beam width). One glint was then masked off to produce the data shown in Fig. 26. Figure 26(a) shows the array formed on each glint when the other one is blocked completely. Figures 26(b) to 26(e) show the increase of power on glint No. 2 as its reflectivity (as measured by its length) is increased relative to that of glint No. 1. The results are summarized in Fig. 26(f) where the ratio of the peak powers on each glint is plotted as a function of the glint reflectivity ratio. The behavior is very similar to the computer simulation results shown in Fig. 7, although the experiment indicates that the glints must be 40% different (roughly 2 dB) in reflectivity for the system to converge on the stronger glint.

The data in Fig. 26 have one unexplained characteristic. The peak power on glint No. 1 does not change as the power on glint No. 2 increases and the sidelobe levels also look much the same. This result is not consistent with constant transmitted beam power, but so far we have no explanation for the observation. The detector was not saturated, and to the eye the power appeared to divide between the glints; it did not jump back and forth.

C. Performance with Laboratory-Generated Turbulence

The experimental arrangement shown in Fig. 18 was used to study the effectiveness of the COAT system in compensating for artificial turbulence generated in the laboratory. The turbulence generator which was placed in one of two identical optical paths consisted of a section of heater tape

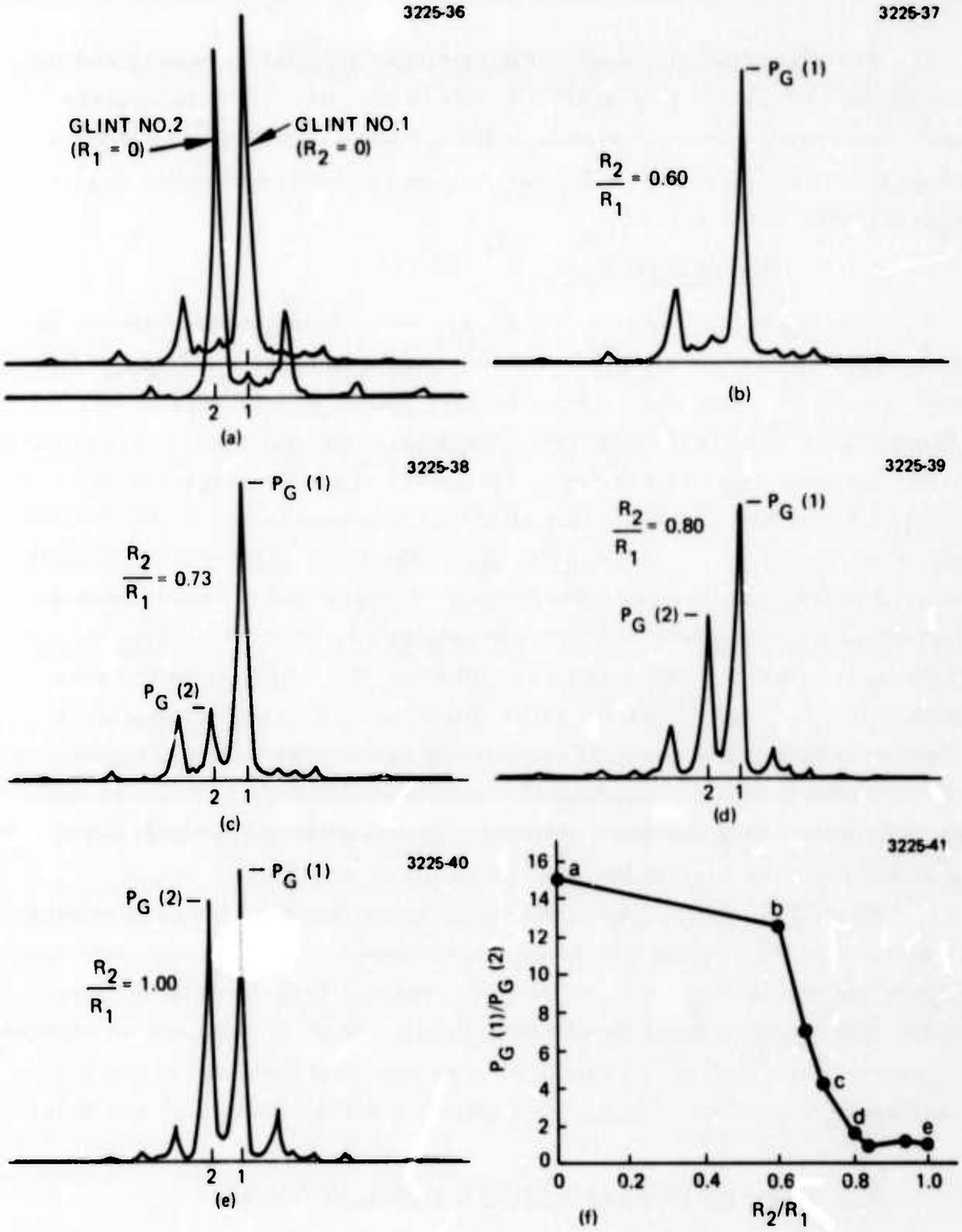

Fig. 26. Two-glint discrimination results using a 1 x 8 linear array. (a) Plots of array patterns for each glint alone. (b)-(e) Reflectivity of glint No. 2 increases. (f) Summary of results.

underneath a copper mesh and a small fan above the mesh to aid in breaking up the generated turbulence. The fan was run at a slow speed so the time variations of the turbulence would not be too rapid.

The test results are presented in Fig. 27. The beam pattern photographs on the left side of the figure show the beam in the nonturbulent path (effectively the input beam to the turbulence) and the beam after it passes through the turbulence. The profiles in the right-hand pictures show the intensity profile through the center of the beam patterns. The pictures indicate that the COAT system stabilizes the beam pattern and provides a factor of two increase in the peak intensity. The COAT-formed beam (Fig. 27(b)) is almost identical to that observed with the turbulence turned off; the only difference is that small fluctuations in the peak intensity occur with turbulence. As discussed in an earlier section, this test rather than a loop open/loop closed comparison is the proper measure of COAT performance, since it indicates the deviation from a perfectly formed beam. The test also indicates the "strength" of the turbulence, which in this case causes a factor of two loss in peak intensity and an unstable beam profile.

The excellence of the COAT performance, both with and without turbulence, cannot be fully appreciated without observing it in action. A movie sequence has thus been made which illustrates the 18-element system performance in the laboratory with and without artificial turbulence. The film shows performance with single and multiple moving glints, black hole tracking, and sphere tracking. The movie was also used to record the excellent performance of the offset-pointing system in both mechanical and electronic modes. Tracking performance while offset-pointing has been demonstrated. The movie was presented as part of an invited talk at the 1974 Spring Meeting of the Optical Society of America.[4]

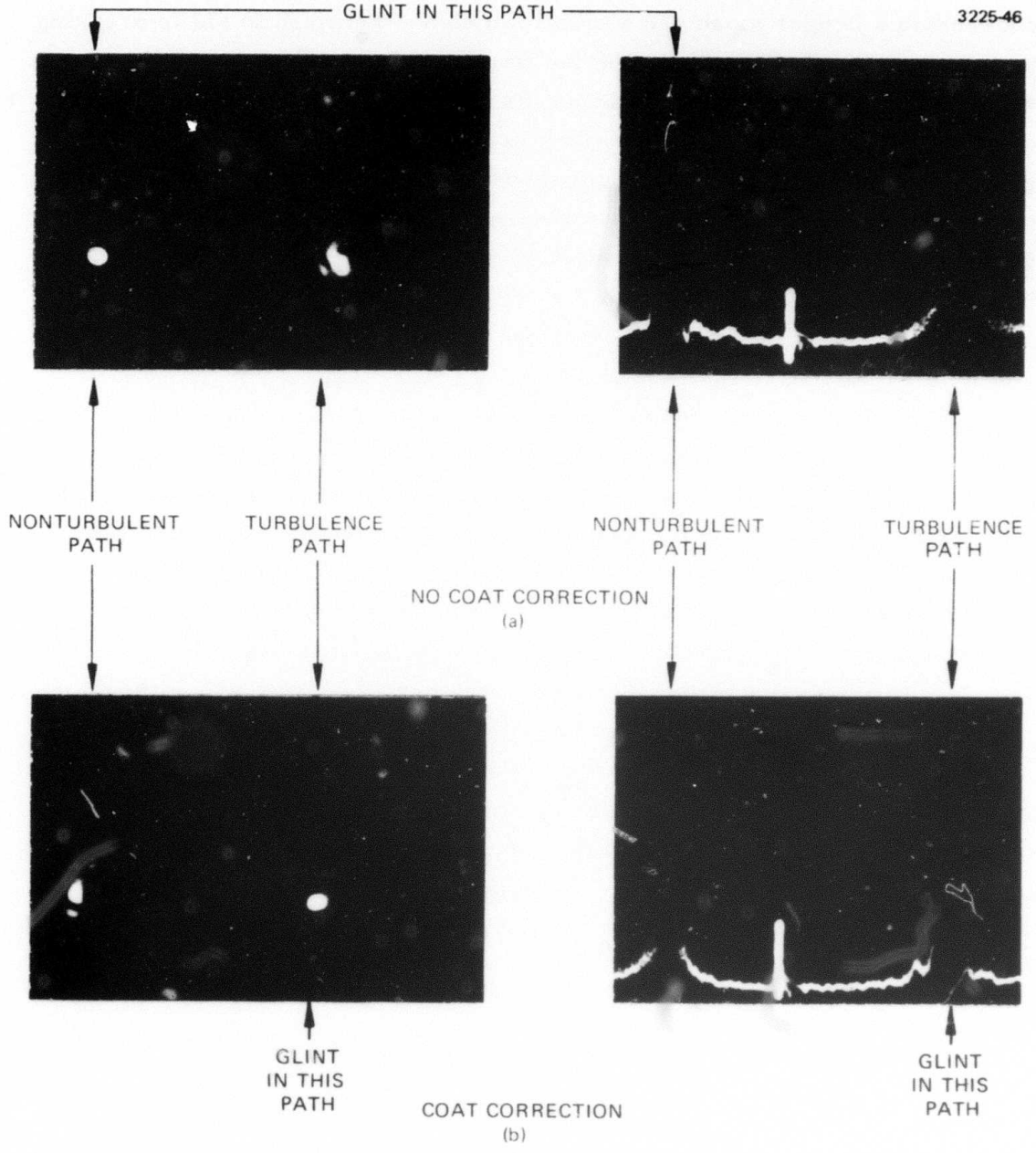

Fig. 27. COAT correction for artificial laboratory turbulence. Left hand photographs show beam intensity patterns for each of two paths (see Fig. 18) and right-hand pictures are profile scans through the beam maxima. (a) Glint placed in non-turbulent path; no COAT-correction for turbulence. (b) Glint placed in turbulent path; COAT corrects for turbulence.

V. RANGE MEASUREMENTS

Preliminary range measurements have been started, but the results will be qualitative until a new TV camera with manual AGC is received. In summary, the system has demonstrated convergence in strong turbulence with single stationary and moving glints and the mechanical offset-pointing has been used with some degree of success. The following sections briefly summarize the test results.

A. Single Stationary Glint

A variation of the laboratory measurements experimental arrangement (Fig. 18) has been used to evaluate the range performance of the COAT system. A schematic of this system is shown in Fig. 28. A local alignment or phasing loop is made using the usual inverted telescope. The "glint", however, is a pinhole with a silicon photodetector behind it. When this detector is selected to provide the phasing signals, the beam to the rooftop range starts out nearly diffraction limited. Any degradation is then caused mainly by turbulence and to a lesser degree, by the imperfect output optics. When phased by this detector, the far field array pattern in the laboratory is shown in Fig. 29(a).

After propagating down the range at a high turbulence level ($C_N^2 = 6 \times 10^{-15}$ cm$^{-2/3}$ = 1.4×10^{-13} m$^{-1/3}$), the beam is degraded to the pattern and profile shown in Figs. 29(b) and 29(c). There is very little difference between these pictures and similar ones taken with the COAT control loop open; the beam has been almost completely dephased.

When the COAT receiver viewing the target is used to phase the transmitter array, the beam forms as shown in (d) and (e) of Fig. 29. The beam forms very well, as can be seen in the photographs. The slight vertical asymmetry seen on the converged beam pattern is caused by a weak second image from the beam splitter in the target assembly.[2] When the system is converged, the control voltages applied to the element phase shifters fluctuate over a range of ±20 V. For the bimorph phase shifters, this corresponds to a phase shift of ±118°, or about one-third of a wavelength.

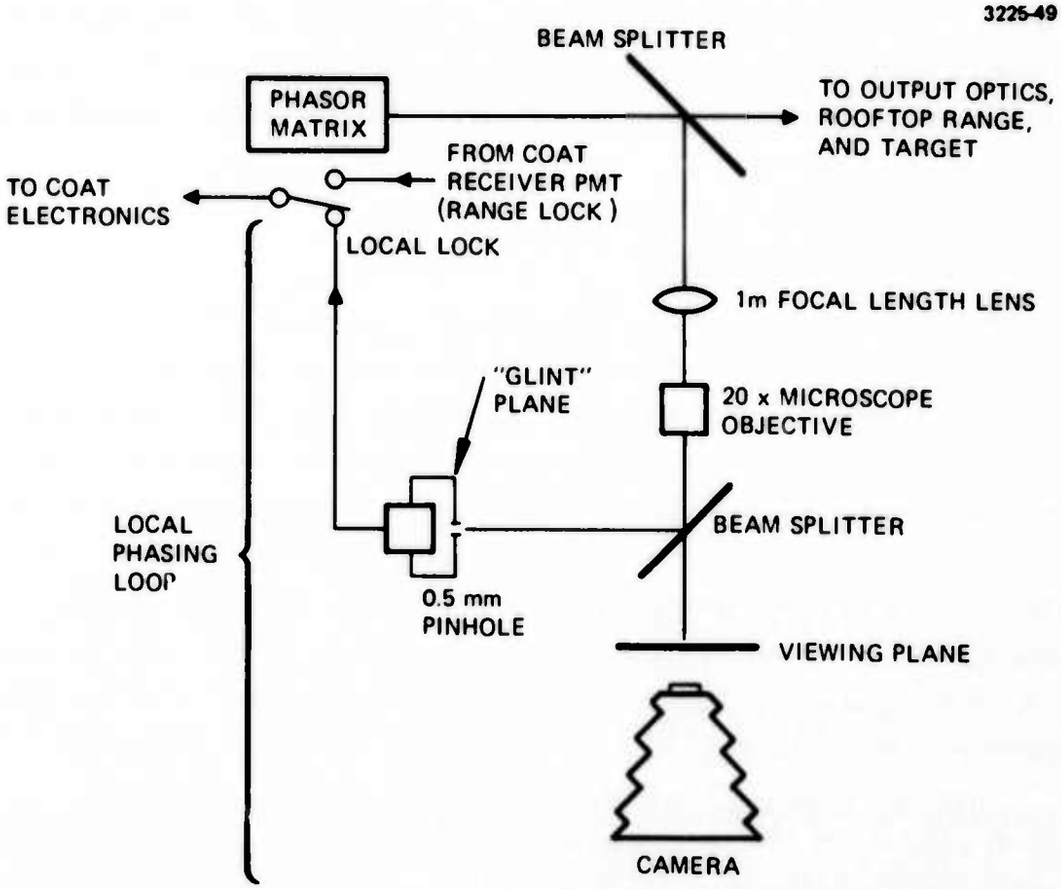

Fig. 28. Experimental arrangement for achieving local phasing loop ahead of outdoor propagation path.

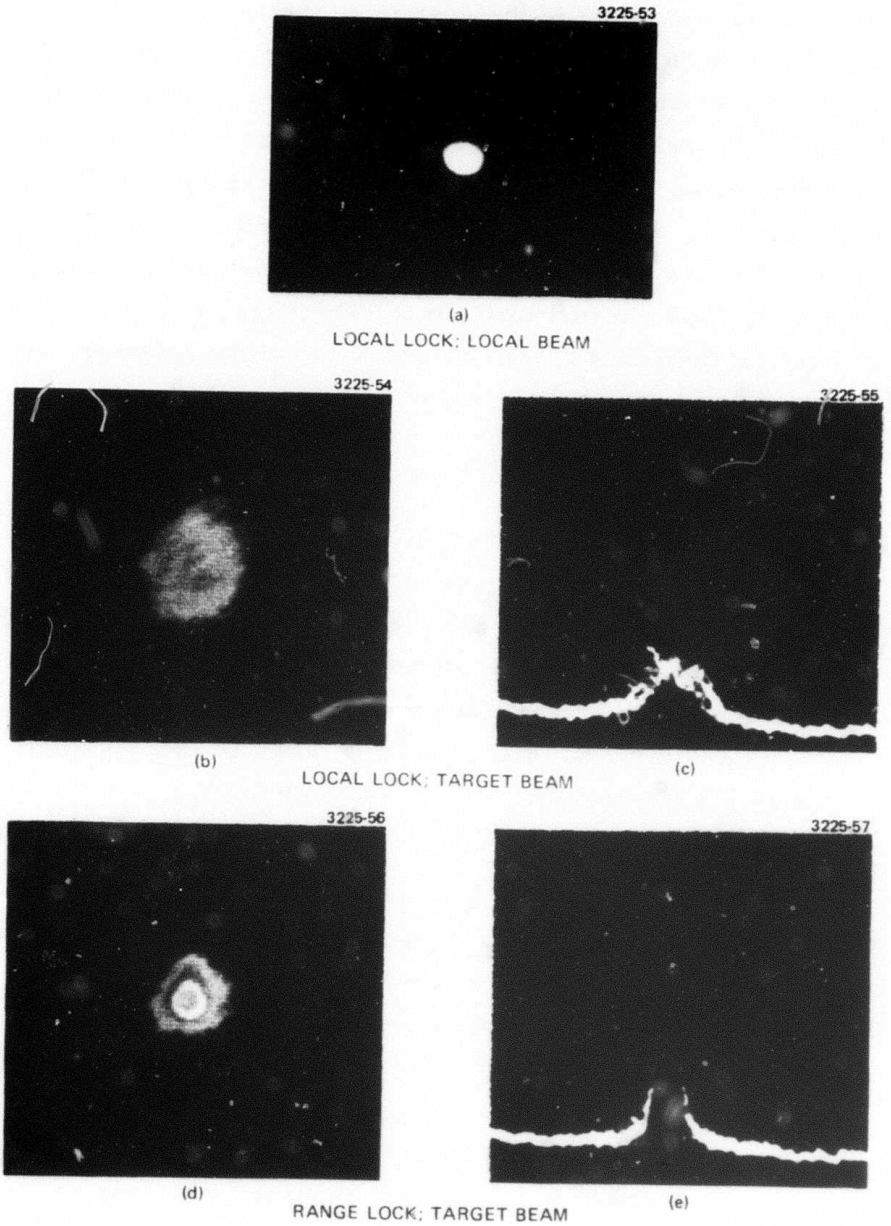

Fig. 29. Range data using local and down-range phasing signals. (a) Far-field pattern of local-loop beam with local phasing signals applied to COAT system. (b) Beam pattern at target with local phasing. (c) Profile scan through (b). (d) Beam pattern at target with down-range (target glint) phasing. (e) Profile scan through (d).

The convergence time of the system on the range with turbulence was measured using the usual COAT PMT receiver. The control loop is closed and the power incident on a target glint is recorded as a function of time. A modified version of glint design No. 1[2] was used; the glint has a 1-mm diameter and an f-number equal to 10. Two convergence sequences are shown in Fig. 30, along with the power on the glint when the array is unconverged. The power on the glint appears to fluctuate by nearly a factor of 2 after the 5 to 7 ms convergence time. This large power fluctuation may be a result of the small detector used in the glint, however, since the fluctuations in the central beam intensity observed with the color quantizer are only 5 to 10%.

B. Single Moving Glint

Video tape data has been recorded which illustrates the performance of the COAT system when a single glint is moved on an elliptical path within the element pattern diameter. The system appears to track the glint with no lag and near-ideal beam formation at rates well in excess of 10 mrad/sec, the contract design goal. No quantitative data on moving glints has been taken as of this writing.

C. Offset Pointing

Only mechanical offset-pointing has been tried so far. The results for an 80 ms sample time and a 200 ms hold period are shown in Fig. 31. The power on the glint varies for most of the 80 ms as a result of mechanical mirror bounce.[1] The beam pattern pictures are photographed off a black and white TV monitor for two different exposures. Qualitatively, the beam is maintaining some degree of convergence, but the average power at the scan point is definitely lower than at the glint point; ideally the average power at the scanned point would be 2.5 times larger. The 200 ms hold time is evidently too long for the strong turbulence conditions existing when this test was run since near-ideal scanning performance has been observed in the lab.[1] Under such strong turbulence conditions, electronic scanning should be better since sample times can drop to 10 ms, allowing the hold time to be reduced to 40 ms for 80% of the average power on the scan point.

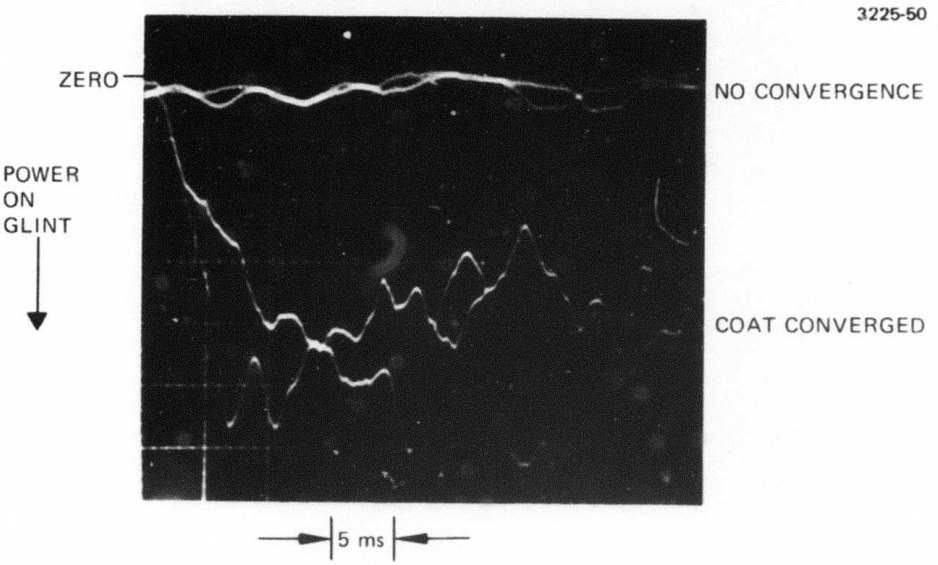

Fig. 30. Convergence data for rooftop range propagation. Two convergence sequences of power on the glint are shown compared to the glint power with no convergence (COAT loop open).

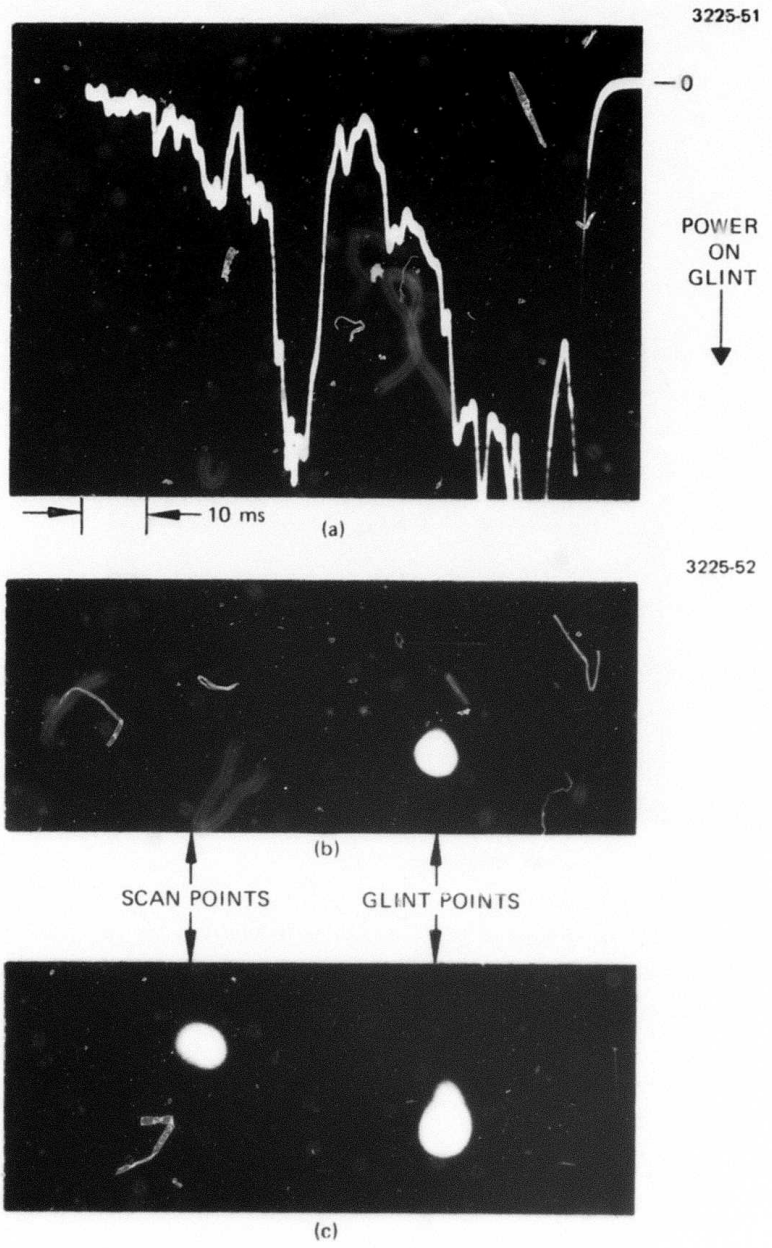

Fig. 31. Mechanical offset-pointing tests under high-turbulence conditions. (a) Power on the glint as a function of time (sample time is 80 ms). (b) Beam pattern at target as seen by the TV monitor. (c) Same as (b), but longer photographic exposure.

VI. PLANS FOR THE NEXT QUARTER

The next quarter will be the last for this program. The completion of the range measurements will include calibrated data on single and multiple glint targets, both stationary and moving, and with different receiver aperture sizes and fields of view. Variations in servo design will also be studied if time permits. A phase correction recording system will be designed, built, and implemented to record the correction voltages across at least four elements of the transmit aperture. These data will be analyzed to determine the amplitude and frequency response required for various targets and for different turbulence levels. Much of the data to be gathered during the next quarter will be dynamic in nature, so most of it will be recorded on tape for later analysis and display.

The additional three month extension of the contract calls for designing a gas cell for use in thermal blooming studies. This design is now in progress and will be completed shortly so that long delivery time components can be ordered.

The high power study program now under way will be finished and reported in a classified addendum to the final contract report.

REFERENCES

1. W. B. Bridges, et al., "COAT" Contract F30602-73-C-248, Report No. 3, January 1974.

2. W. B. Bridges, et al., "COAT" Contract F30602-73-C-0248, Report No. 2, October 1973.

3. W. B. Bridges, et al., "COAT" Contract F30602-73-C-0248, Report No. 1, July 1973.

4. W. B. Bridges, et al., "Coherent Optical Adaptive Techniques," presented at 1974 Spring OSA Meeting, April 1974.